Moderation of high-energy fast neutrons in beryllium from a tokamak fusion reactor and heat transfer to the cooling water system

Benjamin Ellis, PrEng BSc (Eng) *Cape Town* SAIMechE

Supervised by Dr Tom Leadbeater and Dr Tanya Hutton,

Department of Physics, University of Cape Town.

A Minor Dissertation Research Report submitted to the Department of Electrical Engineering, University of Cape Town, in partial fulfilment of the requirements for the Master of Engineering specializing in Nuclear Power.

Cape Town, 27th January 2020

University of Cape Town

The copyright of this thesis vests in the author. No quotation from it or information derived from it is to be published without full acknowledgement of the source. The thesis is to be used for private study or non-commercial research purposes only.

Published by the University of Cape Town (UCT) in terms of the non-exclusive license granted to UCT by the author.

University of Cape Town

Acknowledgements

The author wishes to acknowledge support and guidance of both of his supervisors, Dr Tom Leadbeater and Dr Tanya Hutton, who each assisted in their respective fields to give guidance and encouragement. You both supported me greatly and were always willing to help me when I was struggling with the next step. I am thankful for your kind assistance.

Preface

A modelling demonstration of the moderation of 14.1 MeV primary neutrons in beryllium emitted from a D-T fusion nuclear reaction. The energy deposited from neutron-beryllium interactions which produces heat in the blanket of a fusion tokamak. A review of literature and data available for neutron-beryllium interactions is provided to support the MC software of a simplified model of the ITER first wall and blanket. Energy deposited in regions of the model using FLUKA are used to calculate a polynomial heat flux profile through the model. One dimensional conductive heat transfer through the model is performed and the cooling capacity of the coolant channels via convective heat transfer is explored.

Table of Contents

List of Tables

List of Figures

1 Introduction and overview of study

Nuclear fusion power has always been said to be 30 years away and even longer for it to become commercially scaled but the incredible advantages of being carbon free, the absence of high-level radioactive waste and abundance of fuel has been the dream of scientists. Fusion power has the potential to completely replace fossil fuels as the world's primary energy source and halt the damaging effects of climate change. Though mankind has mastered fission for energy for decades, building hundreds of nuclear reactors, controlling thermonuclear fusion power is technically one of the most challenging fields of experimental nuclear physics. Harnessing the fusion energy has pushed physicists understanding of controlling the fusion reaction, and driven engineers to design new materials and constructions in order to extract the energy emitted (Barbarino, 2018).

In 1997, the European tokamak JET produced 16 MW of fusion power from 24 MW of power injected as heating input (Culham Centre for Fusion Energy, 2020). This is the world record for controlled fusion power with a Q of 0.67. Q is the out-versus-in power amplification ratio. The ITER tokamak is presently the largest and most powerful fusion experiment in the world. It is designed to produce 500 MW of fusion power from a 50 MW heating input. ITER has therefore been designed for much higher fusion power gain, $Q \geq 10$ and this is being achieved by the immense size of ITER's vacuum vessel and the strength of the confining magnetic field, see figure 1. It is planned to be the first fusion device to have a net energy output. ITER will not capture the power it produces as electricity however it will pave the way for future fusion machines that can (Iter Website, 2019).

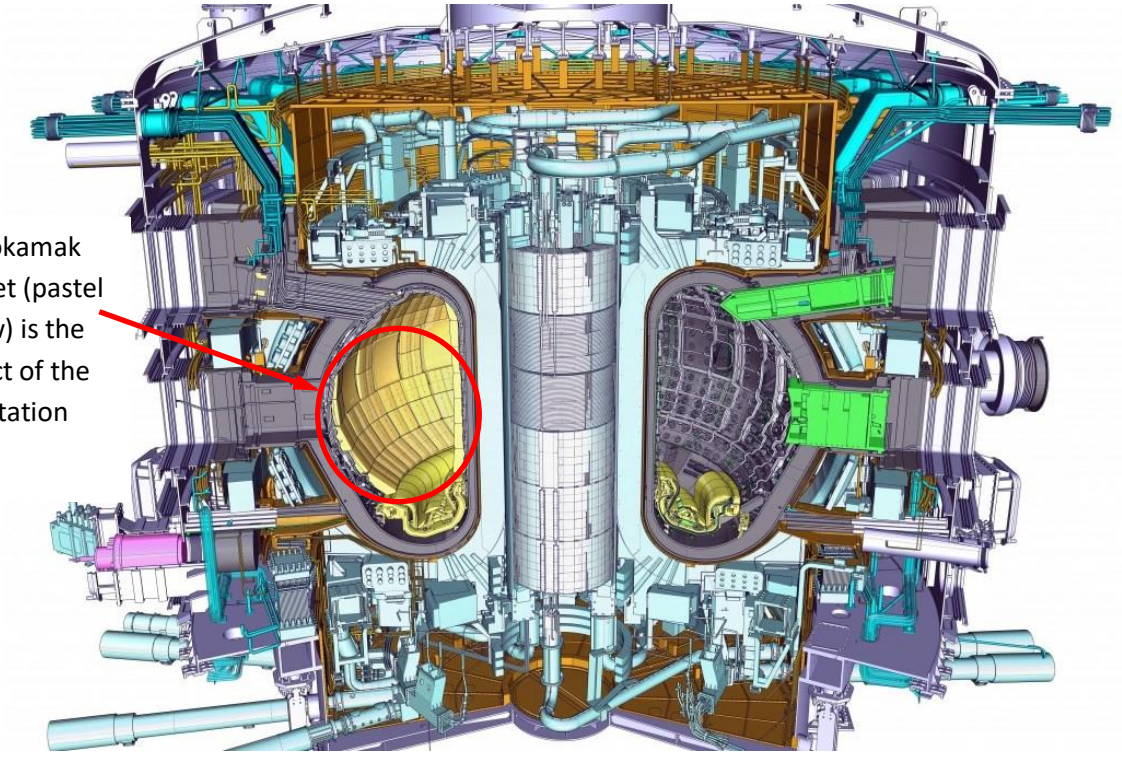

Figure 1: A detailed model of the ITER tokamak (Iter Website, 2019)

The purpose of this dissertation is to demonstrate an advanced level of understanding on the subject. When I started the masters course work I had no knowledge of the ITER project being constructed in the South of France. I became keenly interested in all aspects of its design particularly in the way in which the energy in the nuclear fusion reaction is harnessed. After some preliminary research, I proposed a suitably complex topic, that appealed to me personally as an engineer, who has worked more than a decade in the power generation industry.

The research topic spans several fields of science. It is a journey to explain the source of the thermal heating from the nuclear fusion reaction, and how this energy is transferred into a flowing water that will become high pressure steam needed to drive a steam turbine. The dissertation begins with an explanation of the D-T fusion reaction, the source of primary neutrons and where the neutrons are coming from and where they are going. We will look at the geometry and materials of construction of the First Wall (FW) panel that will be used at ITER. A comprehensive summary of all the main nuclear chain reactions is limited to beryllium, with focus on the Q-values of the reactions. Some discussions on the mechanical issues, gas production namely He and H and fuel breeding (tritium production) are explored.

Connecting the field of nuclear physics with heat transfer is achieved by making use of a Monte Carlo (MC) software package called FLUKA (Alfredo Ferrari, 2018). FLUKA can simulate nuclear processes and score the energy deposited from nuclear reactions due to a neutron flux in a simplified model of the FW panel. The results of the MC simulation are used to be able to create an internal heat flux profile through the cross section of the model. Using Fourier's Laws for heat conduction in a simplified slab, it is possible to estimate and create a temperature profile through 3 sections of the model. The MC simulation also provides data of the neutron fluence in the model enabling one to observe the neutron attenuation. Finally using Newton's Law of Cooling for forced heat convection in a pipe, and using some acceptable assumptions, an estimation of the heat removal capacity of the coolant pipes in the model is calculated.

2 Tokamak fusion reactor geometry and nuclear physics

2.1 Explanation of the fusion reaction

The fuel for nuclear fusion are different light elements, in the case of ITER, the isotopes of hydrogen. The deuterium-tritium (DT) reaction has been identified as the most efficient fusion nuclear reaction as it has been proven in the laboratory to produce the highest amount of energy at the "lowest" temperature. ITER is expected to operate for the first two years with a deuterium-only plasma (DD) allowing the machine to be accessible for repairs, testing the most promising physics regimes and providing an opportunity to test in-vessel tritium breeding blankets in a real fusion environment. Following this, deuterium with a small amount of tritium will fuel the fusion reaction in order to test wall-shielding provisions. Finally, a 12 year long third phase involves an equal mixture of deuterium and tritium (DT) that will be used for full fusion power.

Deuterium is routinely produced for scientific and industrial application. It can be extracted quite easily by distilling water. A single cubic meter of seawater for example can produce up to 33 grams of deuterium. Tritium on the other hand can be found in the atmosphere in trace amounts from the interaction of atmospheric gases with cosmic rays (Iter Website, 2019), and its scarcity is due to the fact that radioactive tritium spontaneously decays to $^{3}_{2}\mathrm{He}$, an electron e^{-} and an electron antineutrino $\bar{\nu}_e$ with a half-life of 12.3 years in the process of beta minus decay (McMorrow, 2011).

$$^{3}_{1}\mathrm{H} \rightarrow {}^{3}_{2}\mathrm{He} + e^{-} + \bar{\nu}_e + 18.6\ \mathrm{keV} \qquad (1)$$

To produce tritium in any quantity it should be "bred" from the interaction of high energy neutrons with lithium contained in the blanket of the tokamak. Sections of this dissertation will discuss tritium breeding from lithium as this is a very important aspect of the fusion reactor.

The focus of this dissertation is the DT fusion reaction as this is the long-term operating regime for ITER. The fusion of a deuterium nucleus with a tritium nucleus (both isotopes of hydrogen) always yields the products of a 3.5 MeV helium ion (α particle) and a 14.1 MeV fusion neutron, as illustrated in figure 2. The nuclear fusion reaction can be described as follows, showing a total Q-value of 17.59 MeV:

$$^{3}_{1}\mathrm{H} + {}^{2}_{1}\mathrm{H} \rightarrow {}^{4}_{2}\mathrm{He} + {}^{1}_{0}\mathrm{n} + 17.59\ \mathrm{MeV} \qquad (2)$$

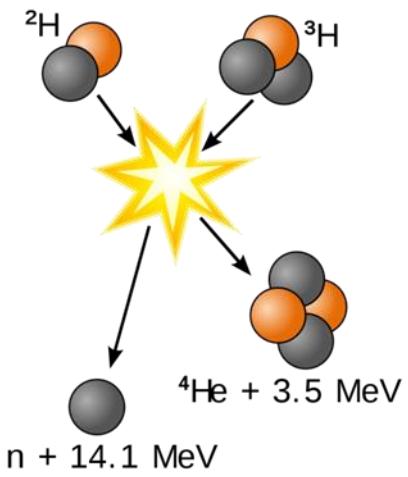

Figure 2: The DT fusion reaction showing the ejection of a 14.1 MeV neutron, diagram courtesy of Wikipedia

Since the nucleus of the hydrogen isotopes have a positive charge, combining the two nuclei will require overcoming the Coulomb barrier. A fusion reaction requires a large amount of starting energy, enough energy to strip the electrons off of the deuterium and tritium. By heating the fuel to 100 million degrees C, the particles accelerate and have enough energy or speed that they form plasma. Within the plasma the particles collide, and the initial electromagnetic repulsion is overcome and the strong interaction binds or fuse together to form a larger atom. The larger atom that is formed in the DT fusion reaction is the helium ion with the single fusion neutron. The combined mass of the fusion products is less than original nuclei and this mass defect equates to a positive Q-value and energy output.

The fundamental nuclear reaction law, conservation of mass plus energy applies and any loss of mass during a nuclear reaction is accompanied by a release of energy, or vice versa. The sum of mass plus energy before and after the reaction are constant. For a detailed calculation of energy released or exothermic reaction of the DT fusion, see Appendix A. Furthermore details of the relative magnitude of the two fusion products from the DT fusion reaction can be seen in Appendix B.

In the fusion power reactor, the helium ions stay within the plasma as they are magnetically confined by the tokamak magnets. The production of each helium ion (3.5 MeV) will contribute to the internal heating of the plasma. It is essential that the helium ions remain confined by the magnetic field until they have transmitted their energy to the fusion plasma, thereafter they should be pumped away as a waste product. The fusion reaction process continues until the plasma is poisoned by excessive impurities or until the heating current stops.

The fusion neutron, which has no electrical charge and is therefore unaffected by magnetic fields is able to escape the plasma. The fusion neutrons, characteristically called the primaries with the

energy of 14.1 MeV, pass through the vacuum vessel and will be moderated and eventually absorbed by the surrounding walls of the tokamak. The process of moderating the primaries, reducing their kinetic energy will result in energy being deposited into the vessel walls, causing the walls to be heated.

An important characteristic of ITER is that the plasma does not burn continuously but has a pulsed operation. It is planned that 3300 pulses, each 400 seconds long will be achieved per year for both DD and DT operation (M.R. Gilbert and J.-Ch. Sublet, 2011). This means that that there will be large intervals of no power or energy output from the fusion reactor. This specific characteristic causes design challenges to accommodate for the thermal expansion of the FW panel as well as the coolant during the pulse period. An active temperature control will be required to maintain constant blanket inlet temperature (Popov, 2011).

2.2 Geometry of ITER tokamak fusion reactor

Most power plants around the world use mechanical power such as a rotating turbine to turn a generator to produce electrical power. The turbine is commonly driven by steam or gas as is the case in coal-fired thermal power stations or gas turbine power stations. In nuclear power stations steam is generated by the heating of the primary coolant from the reactor core. Nuclear power stations harness the energy released from nuclear fission.

The tokamak is type of nuclear power plant that harnesses the energy of nuclear fusion. Within the tokamak, energy is released through the fusion of atoms. Whereas in a conventional nuclear reactor core the nuclear fission reactions primarily heat the fuel rods and are the high heat source, in a tokamak fusion reactor the 14.1 MeV fusion neutron ejected from the fusion reaction enters the walls of the tokamak vessel and causes a multitude of nuclear reactions that summative heats the walls. The walls of the tokamak reactor vessel are collectively called the blanket, while the front-facing elements of the blanket is called the first wall (FW) panel or armor. With ITER, the blanket is designed to remove up to 736 MW of thermal power. The blanket and FW panel are the components of interest of this dissertation.

The ITER tokamak is still under construction, more than 67% complete as of December 2019, with expected first plasma around December 2025. The reactor vessel of the tokamak is a doughnut-shaped vacuum vessel with an external diameter of 19.4 meters and an internal diameter of 6.5 meters. The total height will be 11.3 meters and the volume of the vacuum vessel is 840 cubic meters. The vacuum vessel is vacuum pumped to create low density and will be about one million times lower than the density of air. Inside the vacuum vessel, under extreme heat and pressure, hydrogen gas fuel becomes a plasma. The plasma is a hot electrically charged gas which provides the environment for hydrogen to fuse and yield energy (Iter Website, 2019). See figure 1 for a schematic of the ITER design.

In a tokamak fusion reactor one of the most complicated components is the ‘blanket’, as indicated by the pastel yellow coloured components in figure 1. The blanket is designed to shield the steel vacuum vessel and external machine components from the high-energy fast neutrons produced in the fusion reaction. The blanket surrounds the tokamak and is constructed of elements made up of two parts, the first wall (FW) panels that face the fusion reaction and the shield blocks that carry the heat away. The first wall panels are made of beryllium tiles, 10 mm thick, bonded directly with a copper alloy heatsink layer (Cu-Cr-Zr), 22 mm thick, which is bonded to a back-plate of 316L (N) stainless steel, 49 mm thick (A. A. Badawi, 2004). See figure 3 for a photo of a typical FW panel.

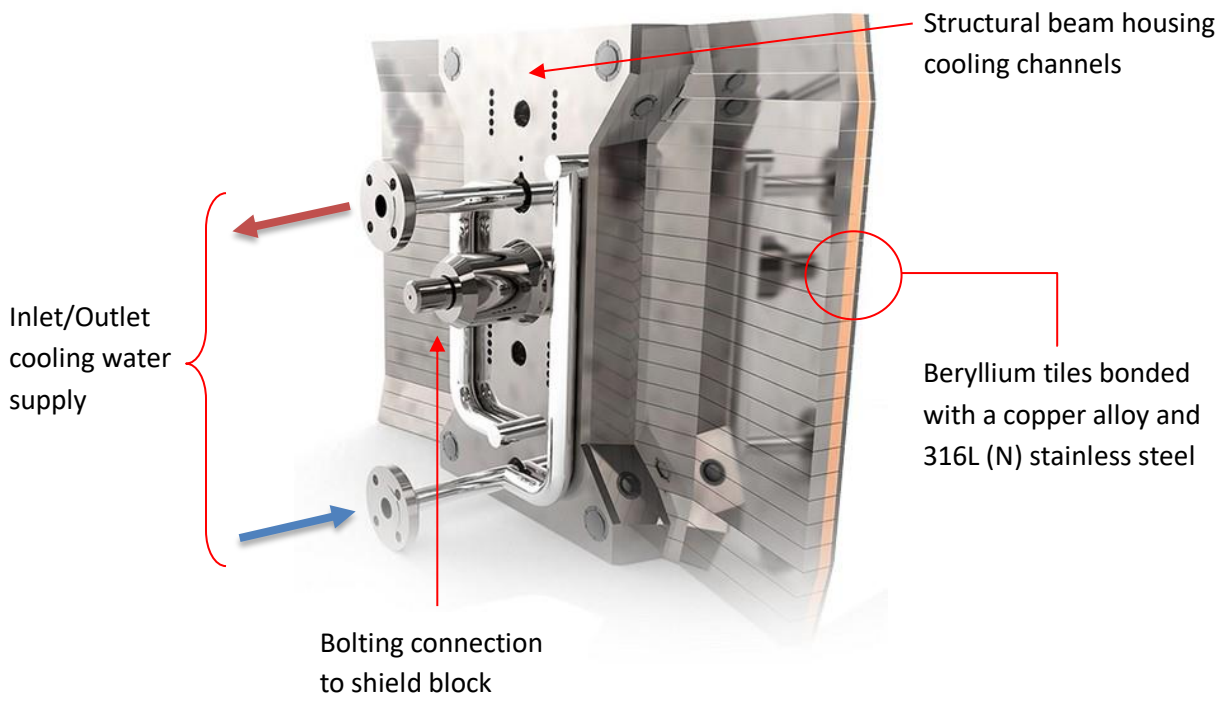

Figure 3: Typical FW panel which will be attached to a shield block (Iter Website, 2019)

On the back of the first wall panels is the shield block, not shown in figure 3. The shield block has cooling water (4 MPa and 70 °C) running through it through manifolds and branch pipes to remove the high heat load expected during operation. The coolant water will be heated by the wall panels and shield blocks through typical thermodynamic heat transfer, which will provide the heat source for a potential steam generator found similar in Pressurised Water Reactors (PWR). The steam vapour from the steam generator would be used to drive a steam turbine which is coupled to a generator to generate electricity (Iter Website, 2019).

2.3 Nuclear reactions with Natural Beryllium

What follows in this section is limited to the interaction of neutrons with beryllium as this is the primary mode of energy transfer within the blanket. Beryllium has been selected as the material of choice for the FW panel of the ITER fusion reactor, due to being a highly effective neutron moderator and having several neutron multiplication reaction channels. These neutron multiplication reaction channels are highly desirable as beryllium will release more neutrons than it absorbs. The net effect is a dramatic increase in neutron flux, in and exiting beryllium, leading to greater capacity for heat generation in the FW panel. Nuclear interactions with the copper alloy, stainless steel and water will not be discussed, however the physical principles (elastic and inelastic scatter) remain the same, but with differing probabilities given by their cross-sections.

The type of nuclear reaction involved depends strongly on:

- The energy of the neutron, in this case the primaries are the fusion neutrons of 14.1 MeV.
- The particular nuclei with which the neutrons collides, in this case natural beryllium of purity 99.9%

The two primary forms of collisions are:

- Scatter - energy from the neutron is transferred to the recoiling nucleus know as elastic scattering or inelastic scattering when the energy from the neutron is transferred to the recoiling nucleus and the nucleus remains in an excited state.
- Absorption - neutron is captured by the nucleus (Peterson, 2018).

Neutron elastic scattering is the first primary form of neutron collision and occurs when a target nucleus emits a single neutron after a neutron-nucleus interaction. There is usually some transfer of kinetic energy from the incident neutron to the target nucleus. The target nucleus gains the exact amount of kinetic energy that the neutron loses. The neutron will scatter in a different direction and the target nucleus moves away at an increased speed. For elastic scattering the energy of the neutron is mostly less than 10 MeV. For neutrons greater than 10 MeV, for example the primary 14.1 MeV neutrons their first couple of collisions with the beryllium may be of sufficiently high energy to excite the beryllium nucleus. Such a collision is inelastic, since some of the kinetic energy is transformed to potential energy by exciting some of the internal degrees of freedom of the nucleus to form an excited state. The maximum energy lost per collision occurs when the target nucleus has unit mass and tends to zero for heavy target elements. Low atomic number (Z) is therefore a prime requirement of a good moderator. Since beryllium Z = 9 is a light material, as explained in this section of neutron moderation, beryllium is very effective at slowing down neutrons through a series of elastic collisions.

Due to the design of the ITER tokamak, it is desirable that the moderator is a solid in the working temperature range for thermal heat transfer. Also, it is required that the moderator remains intact whilst under the vacuum of the tokamak vessel. Therefore, a moderating gas would not be desirable as the gas would diffuse into the vacuum space. Furthermore, gases have a very low number density to have a significant impact on the moderation of neutrons.

Nuclear characteristics of solid Moderators by neutrons						
	Material					
Nuclear characteristics	Li-6	Be-9	B-10	C-12	Na-23	U-238
Atomic or molecular weight (u)	6	9	11	12	23	238
Density (g / cc)	0.534	1.85	2.08	2.26	0.97	19.1
Number of atoms or mole/ cm^3, $*N_A$	0.54	1.24	1.14	1.13	0.25	0.48
Scattering cross section (b), σ_s (0.025eV)	1.03	6.1	2.25	4.81	3.39	9.37
Absorption cross section (b), σ_a (0.025eV)	940	0.009	3409	0.003	0.53	2.42
Macroscopic absorption cross section Σ_a, cm^{-1}	50.39	0.0011	388.25	0.0003	0.0135	0.1170
Macroscopic scattering cross section Σ_s, cm^{-1}	0.0552	0.7552	0.2563	0.5456	0.0861	0.4529
Log mean energy loss / collision, ξ	0.2990	0.2066	0.1713	0.1578	0.0845	0.0084
Slowing-down power SDP, $\xi*\Sigma_s$	0.0165	0.1560	0.0439	0.0861	0.0073	0.0038
Moderating ratio MR, $\xi * \Sigma_s/\Sigma_a$	0.0003	140.03	0.0001	252.96	0.5404	0.0324
Collisions 14.1MeV to 0.025eV	67	98	118	128	238	2405

Table 1: Nuclear characteristics of solid Moderators by neutrons, table adapted from Table 3.1 (Lewis, 2008)

Table 1 (Lewis, 2008) shows the values of the nuclear properties of beryllium, as well as other low atomic weight solid moderating materials. The table represents the five lowest atomic weight solid moderators which will remain as a solid moderator under the heat flux in ITER's first wall panel. Uranium 238 is added to the table for interest and comparison of a heavy atomic weight material. To be an effective moderator a material must have a low atomic or molecular weight. Only then is the average logarithmic energy loss per collision ξ, large enough to slow neutrons down to thermal energies with relatively few collisions. One may assume that Lithium-6 is the best moderator in table 1 due to having the largest slowing down decrement ξ, however a good moderator must possess additional properties namely a high macroscopic scattering neutron cross section and a low macroscopic absorption cross section.

The most complete measure of the effectiveness of a moderator, is the moderating ratio (MR). The moderating ratio takes the ratio of the macroscopic slowing-down power SDP, to the macroscopic absorption cross section. Thus the higher the MR, the more effective the material is to perform as a moderator. Beryllium and carbon are attractive solid moderators as can be seen in the table, with moderating ratios of 140 and 252 respectively. The question then is why is beryllium being used as a solid moderator in the FW armour, when it is around 300 times more expensive than carbon? While beryllium has slightly better thermal conductivity, see table 5, the primary reason is due to beryllium having a very low threshold for neutron emission, a very good neutron multiplier and neutron

source, see section 2.3.7, whereas the same cannot be said for carbon. Due to carbon-12 nucleus being significantly more stable, having an average binding energy of 7.6 MeV per nucleon versus beryllium-9 with an average binding energy of 6.4 MeV per nucleon, larger incident particle energies are needed to induce nuclear reactions with carbon-12. In fact, it can be seen on the ENDF/B-VIII.0 library that the neutron induced cross sections for carbon-12, specifically for neutron multiplier and neutron source have a neutron energy threshold of > 20 MeV. Since the primary fusion neutron is only 14.1 MeV, the probability of carbon-12 being a neutron multiplier and neutron source is nil.

Beryllium as a moderator is also able to produce a small build-up of tritium (predominately via Lithium-6) under a neutron flux, see section 2.3.5. Tritium as mentioned is the fuel for the D-T fusion reactor and is always in high demand due to its extreme rarity. As tritium has a half-life of 12.3 years, there is the possibility to harvest the tritium from the beryllium FW armour after five full years of full-power operation. The replacement of the beryllium FW armour is actually more of a structural requirement because of beryllium swelling discussed later. Carbon on the other hand has a neutron energy threshold of almost 20 MeV for tritium production, making the possibility of tritium production impossible under a neutron flux of 14.1 MeV neutrons and less. Therefore, the advantages of beryllium over carbon as the moderator of choice for ITER is because beryllium produces much more favourable nuclear reaction products.

Figure 4 provides a reference of all the neutron induced nuclear interactions with Beryllium, these are labelled Chains 1 through to 7 (Tomberlin, 2004). Examination of the reaction chains in the table reveals that helium is a reaction product in every chain. The significance of the production of helium results in a gradual build up of helium within the beryllium. It is well recognized that the helium build up in irradiated beryllium is associated with swelling and changes in the mechanical properties of beryllium. Even at low concentrations the helium gas particles can have severe life-limiting consequences for beryllium due to helium's low solubility in the crystal lattice, forming clusters and accumulating at defects, dislocations and grain boundaries. The result of long-term irradiation leads to beryllium swelling and embrittlement, which will be severe due to ITERs unprecedented high neutron fluxes.

Chain 0

Be9(n,n')Be9 14.1 MeV ≈ 1 b

1 MeV ≈ 3.34 b

n(th) ≈ 6.5 b

Chain 1

Be9(n,ɣ)Be10

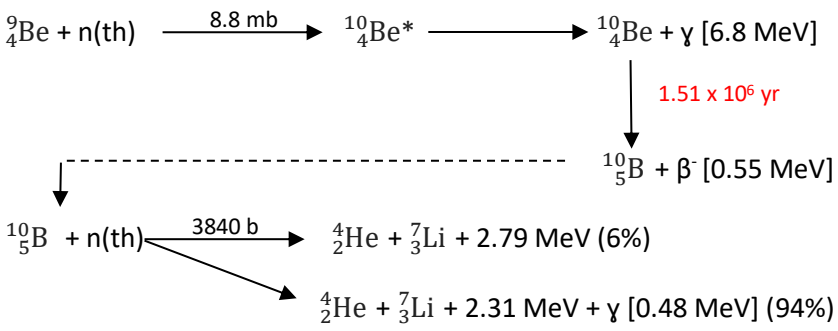

Chain 2

Be9(n,α)He6

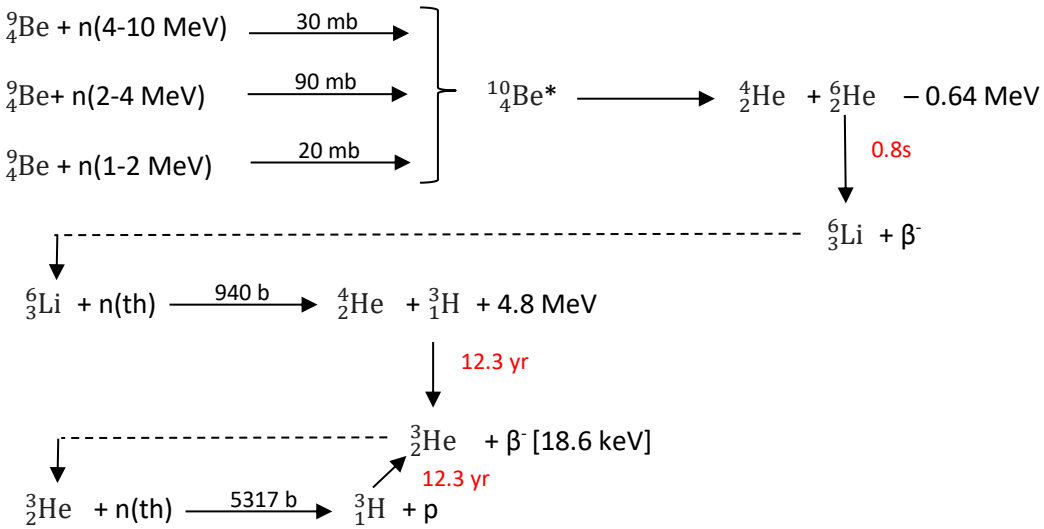

Chain 3

Be9(n,2n)Be8

$^{9}_{4}Be$ + n(>2 MeV) $\xrightarrow{500\ mb}$ 2 $^{4}_{2}He$ + 2n – 1.666 MeV

Chain 4

Be9(ɣ,n)Be8

$^{9}_{4}Be$ + ɣ(>1.67 MeV) $\xrightarrow{1\ mb}$ 2 $^{4}_{2}He$ + n – 1.666MeV

Chain 5

Be9(p,n)B9

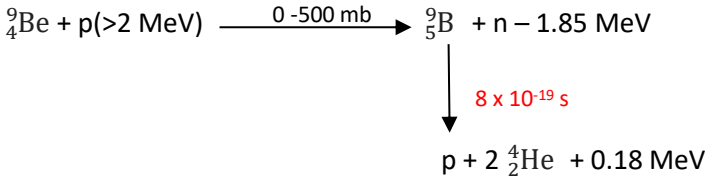

Chain 6

Be9(α,n)C12

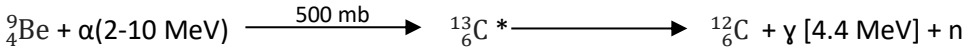

Chain 7

Be9(α, n+α)Be8

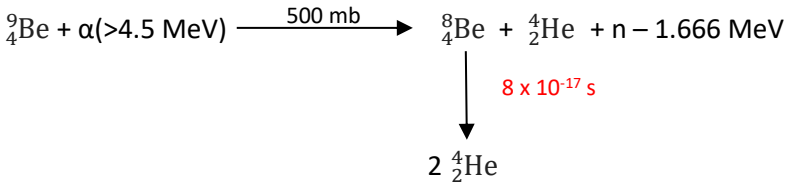

Figure 4: Nuclear reactions with Be-9 (Tomberlin, 2004)

In a fusion reactor, the various components surrounding and facing the plasma will be subjected to much higher neutron fluxes and higher average neutron energies when compared to a fission reactor. Typical fission reactors have an average neutron flux of 3.11×10^{13} n/cm^2/s and mean neutron energy of 2 MeV whereas ITER is predicted to have an average neutron flux 2.38×10^{14} n/cm^2/s and emit a 14.1 MeV high energy fusion neutron from the plasma. The cross sections for some interactions may be negligible in a fission reactor however due to the one order of magnitude difference in neutron flux in a fusion reactor, these smaller cross sections even 1 mb, will have a significant impact. Such high neutron fluxes in a fusion reactor, will cause atomic displacements within the materials, leading to the accumulation of radiation defects – causing hardening, embrittlement and irradiation creep. The aforementioned initiates non-elastic nuclear reactions that cause transmutation or burn-up, changing the chemical composition of the materials, leading to a measurable change in structural and mechanical properties. This will be on a scale not seen in present neutron systems (M.R. Gilbert, 2012).

Even by using special designed fusion materials, it is expected that the blanket of a fusion reactor would not survive the full life of the reactor. The life of a FW panel in ITER is planned to be 15,000 cycles, with each cycle being a pulse about 400 seconds long, estimated 3300 pulses annually, therefore the blanket will have to be replaced every 2 to 5 years. Performing this major intervention would require remote handling operation since the materials of the blankets and reactor vessel will

be strongly activated due to the relatively short half life isotopes (Technical Developments for Harnessing Controlled Fusion, 2011).

2.3.1 Thermalization of neutrons with Beryllium [Elastic Scattering] (Chain 0)

Beryllium has a large elastic scattering cross section Be9(n,n')Be9 for the primary 14.1 MeV fusion neutron, about 1 barn. The elastic scattering cross section continues to increase to 3.34 b for 1 MeV neutrons and to around 6.49 b for thermal neutrons (0.025eV). At very low energies less than 1 meV the cross section is expected to double to 13 b. See cross section plot 1 below (green line), for details.

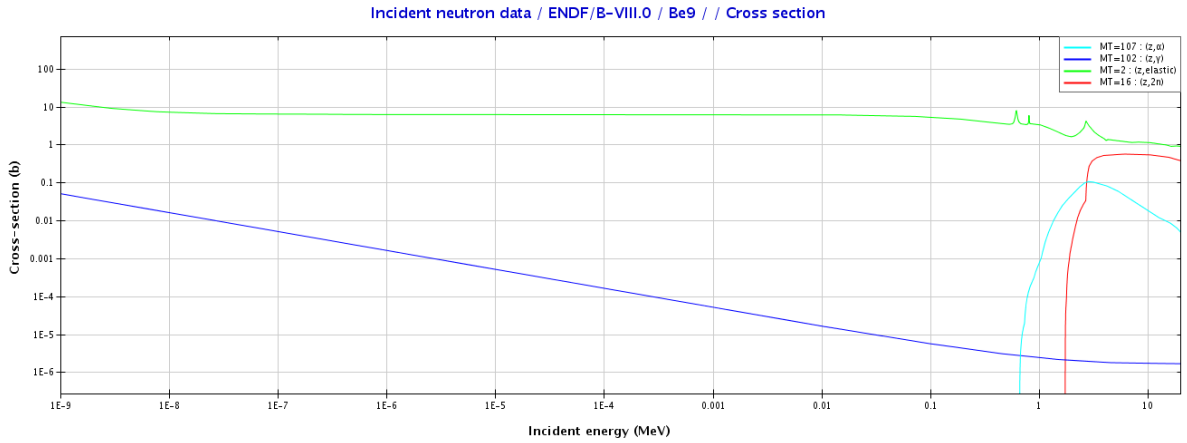

Cross section plot 1: Neutron induced cross section with Be9 (z,α;γ;elastic;2n), Hale, G., et al. (2009). ENDF/B-VIII.0 MAT 425 (D.A. Brown, 2018)

Due to the large scattering cross section, beryllium works as an effective neutron reflector and neutron moderator. In fact, beryllium is often employed as a neutron reflector on fission reactors in order to bring a subcritical mass of fissile material critical, or increase the amount of fission that a mass will undergo.

The effectiveness of beryllium is very dependent on the size of the crystals in the material structure as well as the purity of the metal. Coarse grained beryllium as a possible result of a heat treatment process can have large crystals that can be twice as transparent as small-grained material for low neutron energies. The operating temperature of the beryllium will also have an effect on the cross section. High purity beryllium (so called reactor grade beryllium) is required so that it can be used as a moderator. Small amounts of impurities will have a negative effect and increase the thermal neutron absorption cross section considerably.

A closer examination of the cross section for scatter shows 3 peaks, pointed out in cross section plot 2, which further enhance the moderation properties of beryllium. The resonance peaks have twice the cross section for neutrons at energies adjacent to the scatter peaks and are similar to the thermal neutron cross section of 6.5 b. These resonance peaks will play a significant role in increasing the thermalization of neutrons as they scatter through these resonance peak energies. The resonance peaks can be observed at the following neutron energies:

- The peak is located at 2.72 MeV having cross section of 4.1 b
- The peak is located at 811 keV having cross section of 5.8 b
- The peak is located at 621 keV having cross section of 7.76 b

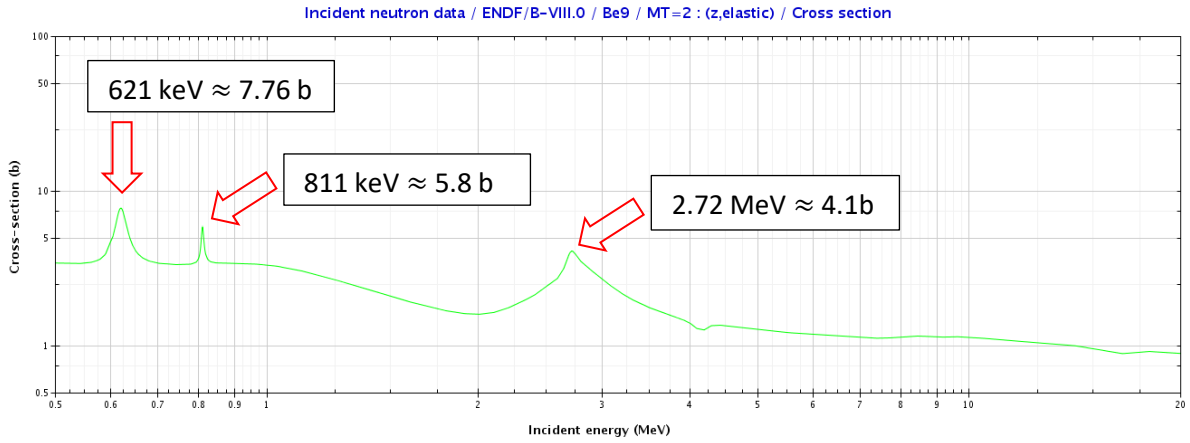

Cross section plot 2: Neutron induced cross section with Be9 (z,elastic), Hale, G., et al. (2009). ENDF/B-VIII.0 MAT 425 (D.A. Brown, 2018)

2.3.2 Thermalization of neutrons with Beryllium [Inelastic Scattering] (Chain 0)

Beryllium also has the possibility to undergo inelastic scattering Be9(n,n')Be9*, whereby some energy from the incident neutron is absorbed to the recoiling nucleus and the nucleus remains in the excited state. Beryllium then gives up the excitation energy by emitting one or more gamma rays to reach its ground state. As mentioned earlier the inelastic scattering reaction is more likely to occur at greater than 10 MeV incident neutron energy. This is shown evidently in the cross section for inelastic collision, where a threshold energy of 3 MeV is required for much higher probability, and at 10 MeV to the 14.1 MeV the cross section is consistently around 0.51 barns. The cross section for inelastic scattering is of significance for high energy neutrons and heavy nuclei where it plays an important role in the moderation of neutrons, however for light nuclei like beryllium, inelastic scattering has a relatively small cross section.

2.3.3 Beryllium as gamma production and Li-7 (Chain 1)

The first nuclear reaction to be observed with natural beryllium is the (n,γ) resulting in a possible thermal neutron activation of Be9 to form the unstable Be10 which promptly emits a 6.8 MeV gamma. The cross section for this can be seen cross section plot 1 (blue line), and scales very accurately as 1/v for energies up to about 10 keV. At thermal neutron energies (0.025 eV neutrons), the cross section is observed to be about 8.8 mb (R.B. Firestone, 2007). This nuclear reaction is heavily reliant on the energy of the incident neutron being in the thermal energy range, neutrons greater than 10 keV are very unlikely to induce this reaction. For higher neutron energy see Chain 2 or 3. For this Chain 1 reaction, the production of a high energy gamma, is defined by the reaction:

$${}^{9}_{4}\mathrm{Be} + \mathrm{n(th)} \rightarrow {}^{10}_{4}\mathrm{Be}^{*} \rightarrow {}^{10}_{4}\mathrm{Be} + \gamma(6.8\mathrm{MeV})$$

The $^{10}_{4}\mathrm{Be}$ is a radioactive isotope with a very long half life of 1.51x10^{6} year. This is can be considered 'stable' however due to the blanket of the ITER fusion reactor expected to be irradiated for a decade, there will be some radioactive decay of $^{10}_{4}\mathrm{Be}$ in this time, which should be considered. Also the neutron flux in the fusion reactor is much higher than in a comparable fission reactor, resulting in higher production of $^{10}_{4}\mathrm{Be}$. The radioactive beta minus decay of $^{10}_{4}\mathrm{Be}$ is as follows:

$^{10}_{4}\mathrm{Be} \rightarrow {}^{10}_{5}\mathrm{B} + \beta^{-}$ (0.55MeV)

The decay product is stable $^{10}_{5}\mathrm{B}$, which in the nuclear industry is commonly used as a neutron absorber due to the high neutron cross section for this isotope. Its (n,α) nuclear reaction cross section for thermal neutrons is about 3840 barns, which can be seen in the cross section plot 3 below. Most of the (n,α) nuclear reactions are accompanied by a 0.48 MeV gamma emission. The two reactions with boron-10 are as follows (Boron 10, 2019):

$^{10}_{5}\mathrm{B}$ + n(th) → $^{4}_{2}\mathrm{He}$ + $^{7}_{3}\mathrm{Li}$ + 2.79MeV (6%)

$^{10}_{5}\mathrm{B}$ + n(th) → $^{4}_{2}\mathrm{He}$ + $^{7}_{3}\mathrm{Li}$ + 2.31MeV + γ (0.48MeV) (94%)

The lithium-7 product of these reaction can be used to produce tritium from a high energy neutron as explained in section 2.3.6.

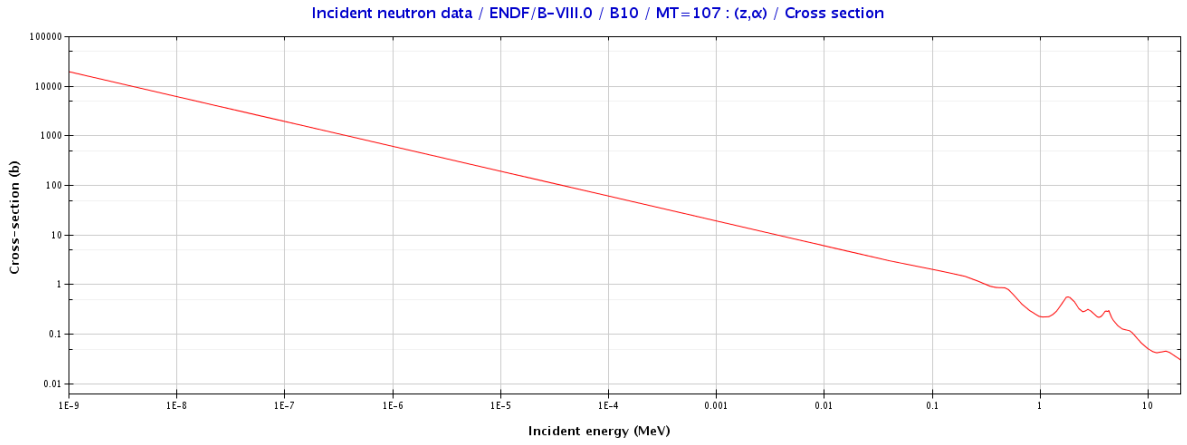

Cross section plot 3: Neutron induced cross section with B10 (z,α), Hale, G., (2018). ENDF/B-VIII.0 MAT 525 (D.A. Brown, 2018)

2.3.4 Tritium production in beryllium (Chain 2)

During extended exposure of the beryllium front wall, there is a small buildup of tritium, specifically when beryllium nuclei absorb neutrons in the 2 to 4 MeV range. An energy threshold of 0.6011 MeV is required for the reaction and its cross section is not constant above the threshold, which makes the potential accumulation of the tritium and helium isotopes very dependent on the neutron energy spectrum. Neutrons with energies between 2 to 4 MeV are to have the highest cross section of almost 90 mb, as can be seen below in cross section plot 4.

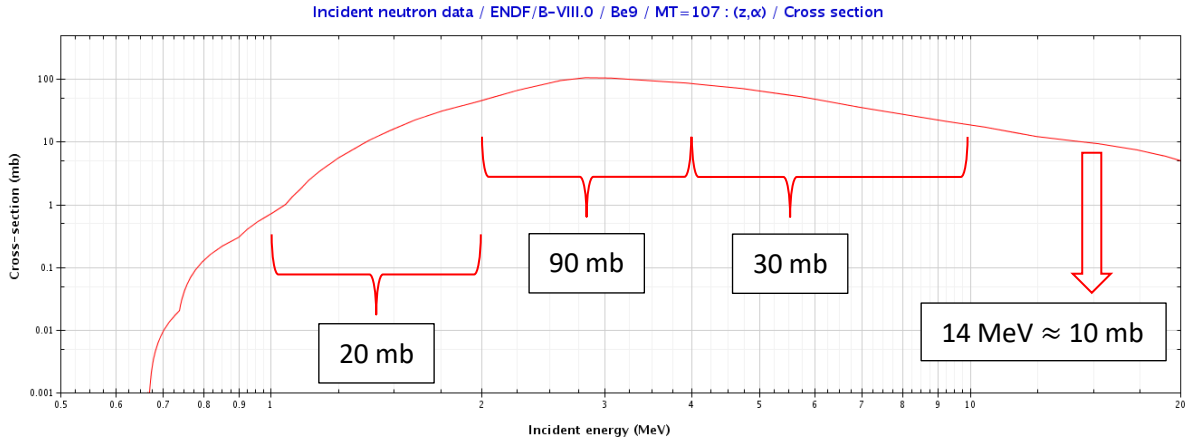

Cross section plot 4: Neutron induced cross section with Be9 (z,α), Hale, G., et al. (2009). ENDF/B-VIII.0 MAT 425 (D.A. Brown, 2018)

The formation of tritium is a 3-step nuclear reaction.

This can be seen in the (Chain 2) reaction: $^{9}_{4}\mathrm{Be} + \mathrm{n} \rightarrow {}^{10}_{4}\mathrm{Be}^{*} \rightarrow {}^{4}_{2}\mathrm{He} + {}^{6}_{2}\mathrm{He}$ **Step 1**

An excited beryllium-10 is produced which immediately breaks down to a helium alpha particle and Hellium-6. The Hellium-6 undergoes rapid beta minus decay to Lithium-6. The half-life of helium-6 is 0.8 seconds.

$^{6}_{2}\mathrm{He} \rightarrow {}^{6}_{3}\mathrm{Li} + \beta^{-}$ **Step 2**

Lithium has two stable isotopes, Li-6 and Li-7, with Li-7 having a natural abundance of 92.5%. It is the Li-6 which is highly valued as a source material for tritium production. The production of $^{6}_{3}\mathrm{Li}$ from He-6 radioactive decay is discussed in the following section.

2.3.5 Tritium production from lithium-6 and buildup of Helium-3 (Chain 2 continued)

Lithium-6 has a large cross section for absorbing thermal neutrons, around 940 b for thermal neutrons. Cross section plot 5 shows that Li-6 scales very accurately as 1/*v* for energies up to about 60 keV. Due to the Li-6's large cross section for thermal neutrons, a carefully designed fusion reactor blanket, with selected materials and geometry in order to minimize loss of neutrons by absorption or escape from the blanket, can potentially slow down the initial 14.1 MeV neutrons to thermal energies and be absorbed by Li-6. Upon Lithium-6 absorbing a thermal neutron, the nuclear reaction results in an alpha particle, a tritium nuclei and a release of 4.8 MeV of energy.

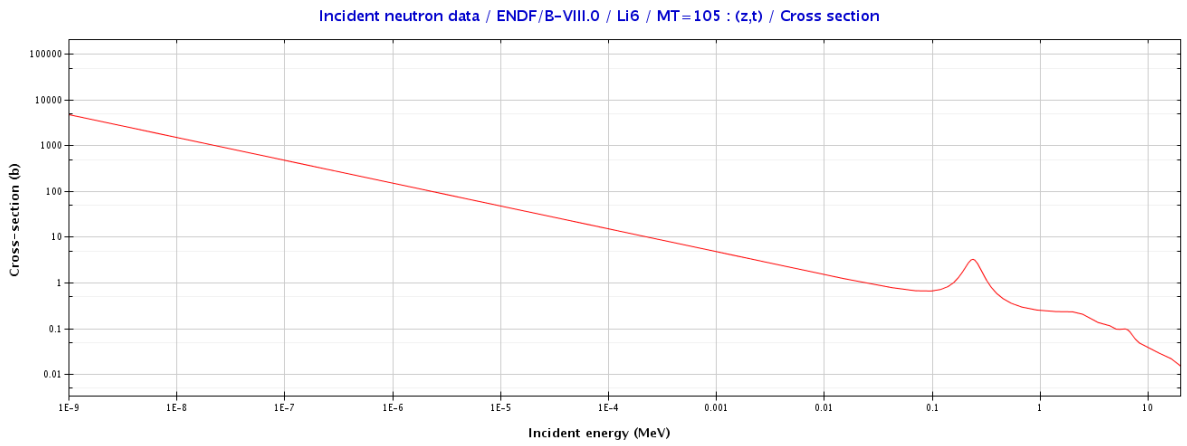

Cross section plot 5: Neutron induced cross section with Li6 (z,t), Hale, G., et al. (2018). ENDF/B-VIII.0 MAT 325 (D.A. Brown, 2018)

Since there is an energy release within wall of the vessel, heat is transferred to the surrounding medium. The nuclear reaction provides a substantial contribution to the thermal output of the fusion reactor, as the energy released, 4.8 MeV is 27.3% of the 17.59 MeV energy release of the primary DT fusion reaction and some 34% of the 14.1 MeV neutron energy actually leaving the plasma.

$^{6}_{3}\mathrm{Li}$ + n(th) → $^{4}_{2}\mathrm{He}$ (2.05MeV) + $^{3}_{1}\mathrm{H}$ (2.75MeV) concluding the production of Tritium. **Step 3**

The initial absorption of the neutrons of beryllium in the 3-step nuclear process will predominately occur in the first centimeter of the blanket, leading to changes in the neutron energy spectrum and flux and thus gas production (H and He). As the lithium is burnt-up (transmuted) in the near-plasma facing regions, fewer neutrons are absorbed and so the flux at greater depths in the blanket increases in the thermal energy ranges over the lifetime of the blanket. The process repeats and continues as the lithium in deeper regions of the blanket is depleted. Over the course of plant operation, Helium production rates in near-plasma regions of the blanket would decrease as the lithium-6 is depleted, while outer blanket regions the Helium production rates would increase as the thermal component of the spectrum in these regions rise and more Li6(n,t)He4 (step3) nuclear reactions take place (M.R. Gilbert, 2012).

Due to extreme rarity of naturally occurring tritium in nature, the synthetic production of tritium using lithium-6 as a source material has been identified for the fusion reactor. Escaping neutrons from the confined plasma will interact with lithium in the blanket or Test Blanket Modules (TBM) which contain an appreciably higher enrichment of lithium-6 enabling the concept of tritium breeding. It has been estimated that a commercial fusion reactor will require about 300g of tritium per day to produce 800 MW of electrical power. As the world's stock of tritium is limited to 20 kilograms that has been accumulated from Candu reactors, it is essential that ITER's tritium breeding development is successful. This is so that ITER can be self-sufficient and be able to produce its own fuel (McMorrow, 2011).

It is very important to note here that in the production of tritium via the chain 2 reaction, that tritium is radioactive with a half life of 12.3 years, see reaction (1). The tritium decays by beta minus to He-3, which has a very large absorption cross section for neutrons, as indicated below in cross section plot 6.

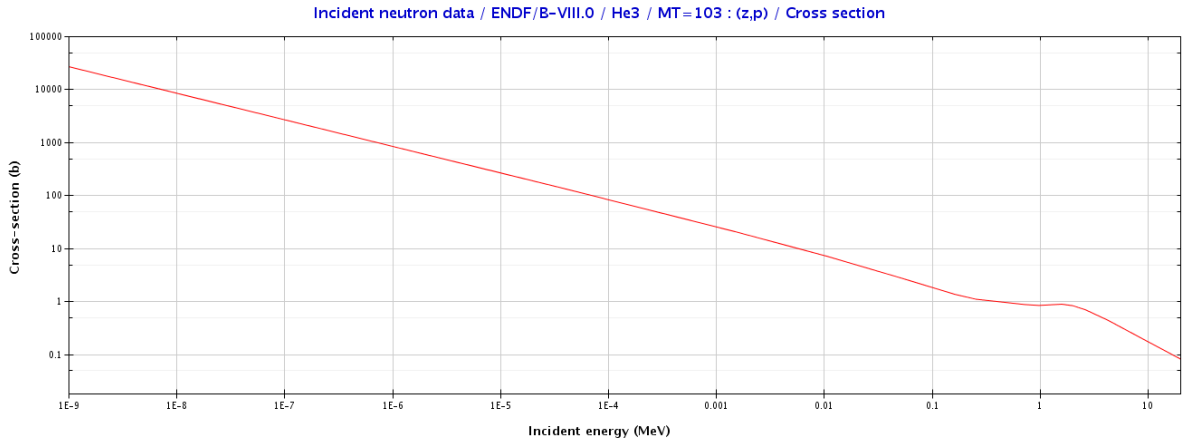

Cross section plot 6: Neutron induced cross section with He3 (z,p), Hale, G., et al. (2018). ENDF/B-VIII.0 MAT 225 (D.A. Brown, 2018)

For thermal neutrons (0.025eV) the cross section is 5317 b. The reaction is as follows:

$^{3}_{2}\mathrm{He} + \mathrm{n} \rightarrow {}^{3}_{1}\mathrm{H} + \mathrm{p}$

Under normal reactor operation, the He-3 is being both generated and depleted, however during reactor outage conditions the depletion ceases. Consequently, during extended reactor outages, the highly irradiated beryllium in the blanket can begin to experience significant increases in He-3 concentrations due to the radioactive decay of tritium.

2.3.6 Tritium production from Lithium-7

ITER plans to use Test Blanket Modules (TBM) which will contain lithium. The blanket will likely contain both stable isotopes of lithium.

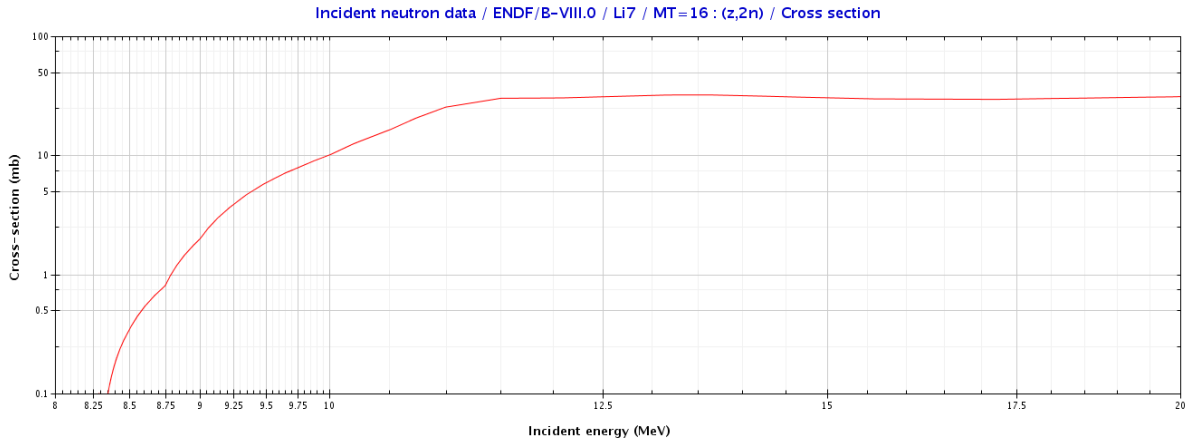

Cross section plot 7: Neutron induced cross section with Li7 (z,2n), Young, P., (2018). ENDF/B-VIII.0 MAT 328 (D.A. Brown, 2018)

As can be seen above in cross section plot 7, a threshold of about 8.3 MeV is required to have the possibility of a Li-7 (n,2n) nuclear reaction. From 11 MeV and greater the cross section is constant hovering around 30 mb. At the primary fusion neutron energy 14.1 MeV, the cross section has been confirmed to be 29 mb.

The reaction is as follows: $^{7}_{3}\mathrm{Li}$ + n (>8.3MeV) → $^{8}_{3}\mathrm{Li}^{*}$ → $^{4}_{2}\mathrm{He}$ + $^{3}_{1}\mathrm{H}$ + n – 2.466 MeV

This reaction was discovered in 1954 when the United States performed a series of high-yield thermonuclear weapon tests called Castle Bravo. The predicted 5 megaton test yielded 3 times due to an error by the designers at Los Almos National Laboratory. The designers had considered Li-7 (accounting for 60% of the lithium content) to be inert. However, this was not the case and the above reaction preceded producing more tritium and an extra neutron. The net result was a much larger neutron flux, greatly increasing the fissioning of the uranium, and ultimately the energy yield (Castle Bravo, 2020).

2.3.7 Beryllium as a neutron multiplier and source

We will discuss 4 different nuclear reactions that yield neutrons as products, these being from neutron, gamma, proton and alpha induced reactions:

2.3.7.1 Neutron multiplication from fast neutrons >2 MeV ***(Chain 3)***

Of the nuclear reactions the one of high interest is the (n,2n) neutron multiplier. A single primary neutron interacting with 9Be undergoes a (n,2n) neutron reaction when the primary neutron energies are greater than 2 MeV to produce Be8, which immediately breaks into 2 alpha particles

and releasing 2 secondary neutrons. Therefore, for neutrons primary or secondary which exceed the 2 MeV threshold, beryllium is a neutron multiplier, releasing more neutrons than it absorbs.

The chain 3 reaction is as follows:

$^{9}_{4}\mathrm{Be}$ + n(> 2 MeV) → 2 $^{4}_{2}\mathrm{He}$ + 2n – 1.666 MeV (endothermic reaction)

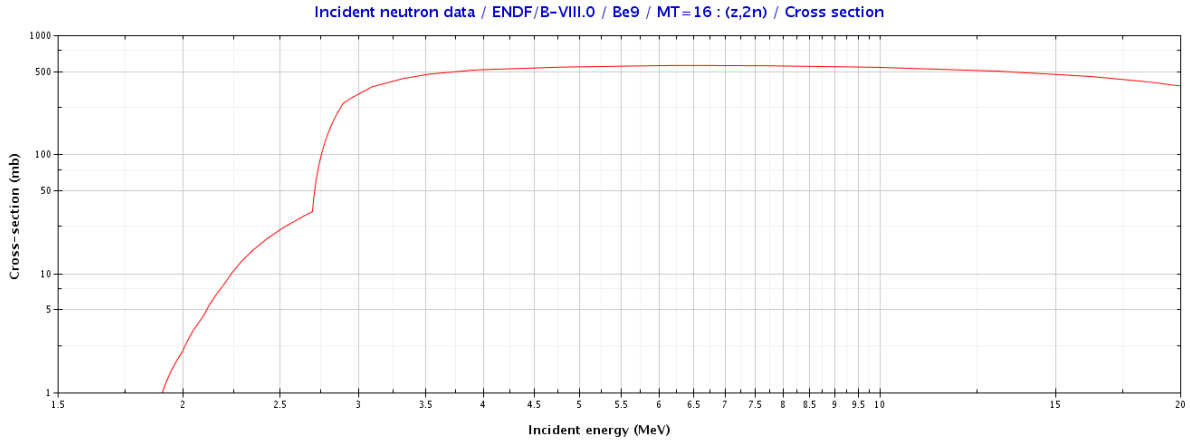

Cross section plot 8: Neutron induced cross section with Be9 (z,2n), Hale, G., et al. (2018). ENDF/B-VIII.0 MAT 425 (D.A. Brown, 2018)

Cross section plot 8 above shows that a 2 MeV threshold can visibly be seen. At greater than 3.5 MeV the cross section is consistently around 500 mb all the way to 13 MeV. For the primary neutrons of 14 MeV, the cross section dips to 486 mb. This nuclear reaction is of much higher probability to occur relatively when compared to other nuclear reactions and it is why beryllium is valued so highly as the FW armor.

2.3.7.2 Neutron source from gamma rays >1.67 MeV ***(Chain 4)***

Another source of neutrons is the (γ,n) nuclear reaction. Any source of gamma radiation for example from chain 1 and greater than 1.67 MeV threshold can result in the reaction. The energy of the gamma radiation must exceed the neutron binding energy of a beryllium nucleus in order to eject a neutron. Other sources of gamma radiation can be from the copper or stainless steel layers which become activated from neutron induced nuclear reactions.

The chain 4 reaction is as follows:

$^{9}_{4}\mathrm{Be}$ + γ(> 1.67 MeV) → 2 $^{4}_{2}\mathrm{He}$ + n – 1.666MeV (endothermic reaction)

The cross section for this reaction is several orders of magnitude less probable than the previous chain 3 reaction, with a cross section around 1mb. Upon Be9 being radiated by a gamma greater than 1.67 MeV, the unstable Be8 immediately breaks apart into to 2 alpha particles and releasing a single secondary neutron.

2.3.7.3 *Neutron source from protons >2 MeV* ***(Chain 5)***

The third neutron source is the (p,n) nuclear reaction, which has a proton energy threshold of 2 MeV. The cross section for this reaction scales with 1/v for energies from 2 MeV to 5 MeV resulting in a cross section from 0 to 500 mb. Sources of protons can be from the highly likely $^{3}_{2}\mathrm{He}$ + n → $^{3}_{1}\mathrm{H}$ + p reaction.

The following describes the chain 5 reaction:

$^{9}_{4}\mathrm{Be}$ + p(> 2 MeV) → $^{9}_{5}\mathrm{B}$ + n – 1.85 MeV (endothermic reaction)

The unstable B9 immediately breaks apart by alpha decay and proton emission. The following describes the reaction:

$^{9}_{5}\mathrm{B}$ → p + 2 $^{4}_{2}\mathrm{He}$ + 0.18MeV (exothermic reaction)

2.3.7.4 *Neutron source from alpha particles 2 to 10MeV* ***(Chain 6 and Chain 7)***

And finally the last neutron source is from the (α,n) nuclear reaction. There are a few possible reactions however they tend to require a high energy alpha particle. The most documented and verified cross section is between 2 and 10 MeV alpha particles which has a cross section of around 100 to 200 mb with almost a 0.5 b cross section peak at 5.74 MeV alpha particles. The following describes the chain 6 reaction:

$^{9}_{4}\mathrm{Be}$ + α (2 to 10 MeV) → $^{13}_{6}\mathrm{C}$* → $^{12}_{6}\mathrm{C}$ + γ(4.4 MeV) + n

The following reaction is alpha induced reaction with beryllium which knocks out a neutron and transmutes the Be-9 to Be-8. This reaction only occurs for alpha particles greater than 4.5 MeV. The following describes the chain 7 reaction:

$^{9}_{4}\mathrm{Be}$ + α (> 4.5 MeV) → $^{8}_{4}\mathrm{Be}$ + α + n - 1.66 MeV (endothermic reaction)

The above Be-8 decays by alpha decay immediately to produce 2 alpha particles as follows:

$^{8}_{4}\mathrm{Be}$ → 2 $^{4}_{2}\mathrm{He}$

The cross section is similar to previous reaction however appears to favor toward higher energy alpha particles. Cross section increases with energy level and plateaus to about 0.5 b at about 8 MeV alpha particle.

A final alpha induced reaction with Be-9 is the following:

$^{9}_{4}\mathrm{Be}$ + α(> 19 MeV) → $^{11}_{6}\mathrm{C}$ + 2n

Since no reaction in the ITER blanket will produce alpha particles greater than 19 MeV the reaction will not occur.

2.3.8 The effect of self-shielding

Accounting for resonance self-shielding is of particular importance due to it strongly affecting the neutrons being preferentially absorbed or scattered out of the resonance energies. Resonances in cross sections can occur that change the likelihood of interaction by one to three orders of magnitude over a small energy range. These resonances are more pronounced and present in heavier nuclei, where the cross section will have significant variations in the epithermal neutron range (E ≈ 0.1eV to 100keV).

Fortunately, the MC code use continuous point-wise cross section data, which allows these resonances to be accurately modeled and accounted for. It can be seen that copper, and the elements of stainless steel do have resonances that are significant and dominant, producing substantial absorption reactions however beryllium being a light nuclei has no resonance peaks and exhibits a smooth profile (Haeck, 2017).

3 Determination of Energy output using Monte Carlo Method

3.1 FLUKA Software

As the reader can appreciate the nature of nuclear reactions that can occur with the transport of particles, with neutrons in particular, in beryllium is immensely complex. Each and every reaction is dependent on 3-dimensions of space, time, and the variables of energy span several decades (from fractions of eV to several MeV). In this dissertation a numerical approach to neutron transport will be used which is based on a probabilistic computer code. The Monte Carlo Method (also called the probabilistic method or the stochastic method), tracks discrete particle histories and averages a random walk directed by measured interaction probabilities. The probability of interaction for all particle energies is based on the cross-section libraries. The nuclear reaction data library that will be used is the ENDF/B-VIII.0 which fully incorporates the new IAEA standards and is the 8th Major Release of the library.

FLUKA was chosen for the dissertation for neutron transport software. FLUKA can be used freely for scientific and academic purposes. The software makes use of probabilistic code that is based on the Monte Carlo Method. The software package simulates nuclear processes. FLUKA stands for FLUktuierende KAskade which is German for “Fluctuating Cascade” and is a general purpose tool for calculations for particle transport and interactions with matter. FLUKA has been developed using the FORTRAN language. The applications of the FLUKA software are wide and can be used for accelerated particle shielding, calorimetry, activation, dosimetry, detector design, Accelerator Driven Systems (ADS), cosmic rays, neutrino physics and radiotherapy (Alfredo Ferrari, 2018).

FLUKA can used to simulate to a high accuracy the interaction and propagation in matter of about 60 different particles including photons, electrons, neutrinos, muons, hadrons, antiparticles, neutrons and heavy ions. FLUKA is able to simulate thermal neutron transport, which many other general purpose codes are unable to do. In the dissertation we shall be using software code for low-energy neutrons (< 20 MeV). For neutrons with energy lower than 20 MeV, FLUKA uses its own neutron cross section library (P5 Legendre angular expansion, 260 neutron energy groups) containing more than 250 different materials, selected for their interest in physics, dosimetry and accelerator engineering and derived from the most recently evaluated data. FLUKA also provides powerful built-in scoring, well tested and suited for most applications.

Due to FLUKA being a complicated software to create and edit input files, execute code and read the output files we used Flair for FLUKA. Flair is an advanced user friendly interface for FLUKA to facilitate the editing of FLUKA input files. Flair provides an easy almost error free front-end interface and works directly with the FLUKA cards using a small dialog for each card. Flair displays the card information in an interpreted human readable way. Flair also has an interactive geometry editor and debugger, along with a library of materials and geometric objects for easier editing (Alfredo Ferrari, 2018).

FLUKA runs in a Linux environment, in this case running on a virtual machine (VM) which is then able to run the FLUKA software code. To run the MC simulations for this dissertation I used Oracle VM VirtualBox which is a free and open-source hosted hypervisor. My supervisor was able to provide me a copy of a virtual hard disk for the VirtualBox which already had the FLUKA and Flair and range of other applications already installed.

3.2 Setting up model geometry

The geometry originally chosen for this dissertation was a simplified model which represents the cross section of the ITER blanket, see figure 3. A neutron beam is generated and orientated directly in front of the model pointing in the positive z-direction as illustrated in figure 5. As in the ITER blanket, the model consists of a sandwich of materials with beryllium as the FW, followed by copper, then stainless steel 316L and finally water. The thickness of each of these layers in the model is 1.0 cm as well as the area is 1.0 cm^2. This simplified geometry for the ITER blanket was used as a learning experience to fully understand how to use Flair and FLUKA. Several runs were made until successful and useful results were obtained. Following this the geometry was advanced to a more realistic FW panel cross-section model.

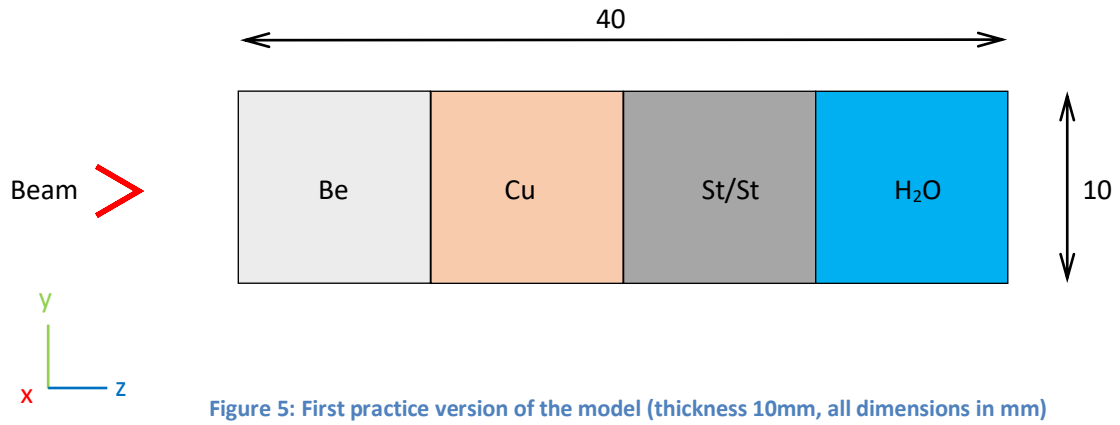

Figure 5: First practice version of the model (thickness 10mm, all dimensions in mm)

A second geometry of the FW panel was modeled in Flair, that represents a repeating unit cell that would make up the entire FW panel. This geometry as shown in figure 6, is much more complex, due to varying thickness of the layers of metal and having columns of water in the copper and stainless steel 316L regions which represent the cooling pipes that will carry away the internal heat generated. This FW panel model with these specific dimensions have been the basis of several evaluations and it was most appropriate and established model to use. Screenshots of the front cross-sectional view, 3-dimesional model and the input code to Flair can be seen in Appendices C to E.

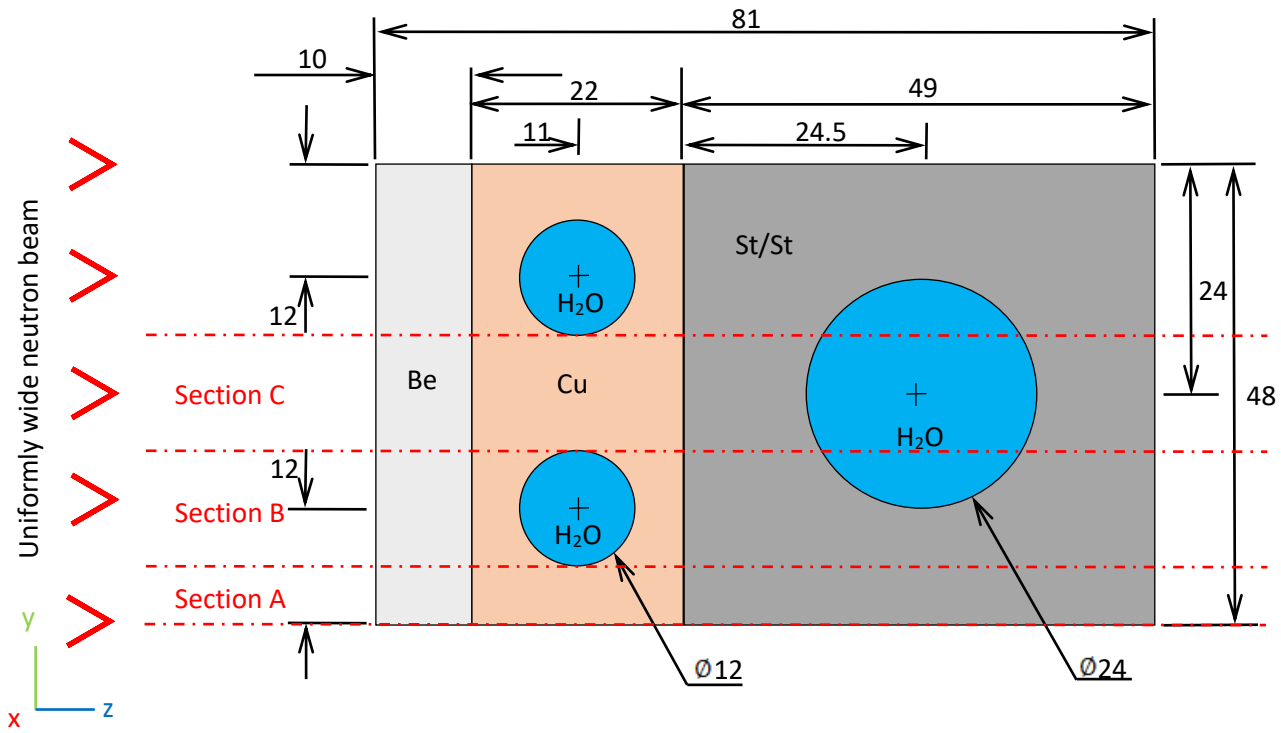

Figure 6: Final version of model used for analysis (thickness 48mm, all dimensions in mm)

In designing the model for FLUKA, it must be appreciated that model represents less than 1% of a FW panel and is but a small repeating unit cell. Performing a MC simulation for an entire FW panel would take an exceedingly long time and require a great deal of computer processing power. In order to accommodate the fact that FW panel is made up of hundreds of unit cells each adjacent to each other, the boundaries of the model used in the simulation were extended by 1 cm in both the x and y-directions. This means that extra material of beryllium, copper and stainless steel was added bringing the front wall cross-section to be 6.8 by 6.8 cm. The three water columns were also extended to match. An uniformly distributed neutron beam was expanded over the entire cross section with Δx and Δy = 6.8 cm. The larger model can be seen in Appendix D. The reasoning for this is to avoid systematic errors in FLUKA from neutron interactions and other particles that may occur on the design model surface. Also by having this extra 1 cm of material which is under a neutron flux, neutrons and other particles and radiation which may have interacted in the extra material can cross into the scored volume. This avoids losses of energy deposition (edge effects) that may have not been accounted for if not modelled in this manner.

3.3 The input file using Flair

A brief description and input cards to the FLUKA input file are discussed, so that one can understand how the MC simulation is setup. A screenshot of the input file using Flair can be seen in Appendix C. Flair uses extended cards for defining the problem input and these cards are grouped into categories. This dissertation has made use of the following cards:

General – The Title of the Simulation is given, and the Default is set to Precision Simulation.

Beam Characteristics – The card describes the primary starting particles. In this card a beam of neutrons of 0.014 GeV (14.1 MeV) with an even distribution in both the x and y plane has been defined. The beam is projected along the z axis.

Beam position – Beam is placed at the co-ordinates (3.4; 3.4; 0.0) cm in the positive z direction. FLUKA uses centimeters for all geometry.

Geometry – A group of cards are used to describe the geometry. These cards are subcategory cards containing bodies, regions and optional region volumes. The input for the Combinatorial Geometry must be immediately preceded by a GEOBEGIN card and immediately followed by a GEOEND card.

In the GEOBEGIN card, the COMBNAME format is selected so that names can be used instead of body and region numbers.

The next card is for the black body. The card describes the geometry for a black body (black hole) which is a sphere with radius 10 meters. This is so that particles that enter the black body are eliminated from the system and so the code stops tracking them to infinity, in other words defines the problem space.

Following card is for a void body. The card describes the geometry for a void (ideal vacuum) which is a sphere with radius 1 meter. This is so that actual geometry is surrounded by a region of ideal vacuum, and to have the black hole region surrounding the vacuum. This is so that the primary particles start their trajectory outside the physical geometry. This closely represents the vacuum vessel of the ITER tokamak.

Next cards describe the physical geometry and the section is titled the Target Sandwich – Three cards describe the geometry for a rectangular parallelepiped body (RPP). The three cards are named according to their material name, these being Be, Cu and StSt. And a further three cards describe the geometry of right circular cylinder body (RCC). The three cards are named H2OA, H2OB and H2OC and are cylinders that are parallel to the x-plane.

It is advised by FLUKA that bodies are not touching at surfaces. This could lead to precision errors in the code. The three cards for the RPP, describing the Target Sandwich have a deliberate forced partial overlap of the bodies by 0.1 cm in the z direction, whereas the RCC for the water columns are defined with regions described below.

Lastly eight cards are used to describe the regions of the geometry. This is done by Boolean zone expressions using + or – operators. Zones are defined by intersections and/or subtraction of bodies. The GEOEND card then concludes all the geometry.

Media – A group of cards are used to describe the material definition and assignment. Each geometry region is to be filled with a homogenous material, or vacuum or black hole. The materials can be simple element, compound, mixture or alloy of known composition. Assignment of the black hole, vacuum, beryllium, copper and water was done easily using a predefined MATERIAL card. For the stainless steel 316L, the material was defined using a COMPOUND card to describe its composition as a mixture. A simplification was made here to represent stainless steel 316L by only three element composition and to ignore various elements of less than 2%. The austenitic chromium-nickel stainless steel is 16% chromium and 10% nickel with the balance being iron. Chromium is not a predefined material and an additional MATERIAL card was used to specify its atomic number Z = 24 and density 7.19g/cm^3.

Scoring – Two cards were used to describe the scoring for FLUKA. Both the cards used USRBIN which places binning detectors independent of the geometry. A cartesian binning mesh was defined for the model. The quantity of total energy deposited, and quantity of total neutron particles were binned.

Set random seed number – A card is used to specify the starting point when FLUKA generates a random number sequence.

The Start and Stop card – Two cards are mandatory in order to actually start the calculation. The START card indicates the number of particle histories requested, in this case the default 1000 was selected. The input file can be closed with the STOP card.

3.4 Scoring and results

Two scorings were performed on the geometry using USRBIN for energy deposition and for neutron flux. Three separate and distinct cross-sections through the geometry, called section A, B and C were scored. The three cross-sections are marked in figure 6. Each of these sections were divided equally into 81 bins for scoring. These bins for all sections were identical in thickness and width, z and x direction respectively however differed in height, y direction. As a result, the bins in section A have a volume of 0.288 cm^3 and the bins in section B and C have a volume of 0.576 cm^3, summarized in table 2. Thus, three sets of results were output for each section and each section had 81 bins. There was no need to perform scoring for the whole FW model as the model is horizontally symmetrical at the midpoint.

FLUKA runs the simulation in cycles, allowing the user to pause, end before completion, add more cycles to an existing simulation etc. while maintaining the same geometry between cycles. At the end of each cycle the output files are copied onto the running directory, the temporary directory is erased and a new one is created where the next run will take place. Originally 5 cycles of 1000 neutrons were used in the MC simulation however initial analysis proved results to be too widely distributed, and the number of cycles were increased.

A total of 20 cycles of 1000 neutrons (20 000 neutrons) were used in the MC simulation and the output files from FLUKA needed to be processed. The output files were readable but not in a format for converting easily into an excel spreadsheet. A short script of Python was used to extract the contents of the FLUKA output file and paste the parsed numbers into a simple text file, a single number per line (Hutton, 2019). As 20 cycles were run in FLUKA over the 81 bins this generated 1620 bins. Each section (A, B and C) had 1620 bins for a total of 4860 bins. Each one of these bin outputs were copied over to an excel spreadsheet. All the above was performed in parallel for energy deposition and for neutron flux, using the same 20 cycles but generating two FLUKA output files which were copied to two separate spreadsheets.

The FLUKA output for energy deposition is expressed in GeV per cm^3 per unit primary weight. While the neutron particle scoring, the neutron flux is expressed in neutrons per cm^2 per second per primary. In both cases the primary is one. Large spreadsheets of the 4860 output data values were analyzed and presented into various graphs as seen in the following section.

3.5 Energy deposition introduction

The primary objective of the model is to calculate the amount of energy deposition in each of the regions of the model. The energy deposited is a summation of all the nuclear reactions within the test model that convert to heating of the model. In order to determine the energy deposited in the regions, FLUKA needs to provide a scoring for energy deposition.

The complex calculations performed by FLUKA of the energy deposited E_{dep}, within a region can be simplified by the following equation:

$$E_{dep} = E_{in} + \Sigma Q - E_{out}$$

Where E_{in} is the energy (excluding mass energy) of the radiation entering the volume (the binned region in FLUKA), E_{out} is the energy of the radiation leaving the volume, ΣQ is the sum of all the Q-values for nuclear reactions that have occurred in the volume. The Q-value is the amount of energy absorbed or released during the nuclear reaction. The nuclear reactions are the ones described in section 2.3 of this dissertation for beryllium. Similar, if not more complex nuclear reactions will take place for the other materials also yielding Q-values however this is beyond the scope of this dissertation. Libraries for Q-values for nuclear reactions can be calculated based on the conservation of total relativistic energy in the basic reaction:

$$m_x c^2 + T_x + m_a c^2 + T_a = m_y c^2 + T_y + m_b c^2 + T_b$$

where the T's are kinetic energies (nonrelativistic approximation is $\frac{1}{2}mv^2$ at low energy) and the m's are rest masses. The Q-value can then be defined as the initial mass energy minus the final mass energy or alternatively the excess kinetic energy of the final products:

$$Q = (m_x + m_a - m_y - m_b)\, c^2 = (m_{initial} - m_{final})\, c^2 = T_y + T_b - T_x - T_a = T_{final} - T_{initial}$$

The Q-value can be positive, negative or zero. A $Q > 0$ ($m_{initial} > m_{final}$ or $T_{final} > T_{initial}$) is an exothermic reaction, a release of kinetic energy in the final products. A $Q < 0$ ($m_{initial} < m_{final}$ or $T_{final} < T_{initial}$) is endothermic reaction, the conversion of initial kinetic energy into nuclear mass or binding energy. An endothermic reaction is an absorption of energy (Krane, 1988).

3.6 Energy deposition in model

The output from FLUKA of the energy deposition is the sum of deposited energy from all nuclear events that occurred within each bin. The raw data can be graphically represented to show the average energy deposition in each section A, B and C, from the front beryllium wall face to the rear stainless steel face in positive z direction. As twenty cycles were run, each with 1000 primary neutrons, the standard deviation σ, of this data set can be calculated as follows for every bin through the section:

$$\sigma = \sqrt{\frac{1}{N-1}\sum_{i=1}^{N}(x_i - \bar{x})^2}$$

Furthermore, the standard error of the mean σ_M, is a method to estimate the uncertainty of a nomalised distribution of results. The standard error of the mean can be calculated as follows:

$$\sigma_M = \frac{\sigma}{\sqrt{N}}$$

With this the statistical precision of the output from FLUKA can be analyzed. An excel spreadsheet can quickly process the data to present some plots of the energy and the standard error through the cross section of the FW panel model. The error bars in the plots, figures 7, 8 and 9 are specified and calculated as:

$$\bar{x} \pm \sigma_M$$

Some immediate observations can be interpreted from the figures 7, 8 and 9. The data has large margins of error and the only way to improve the size of the error is to run a lot more cycles in FLUKA. This will greatly improve the precision. The energy deposited is highest in the front layers of beryllium and copper and reduces to about half by the last layers of stainless steel. It is important to note that the values for energy deposited are normalized in terms of the energy of a single 14.1 MeV fusion neutron. In order to have real life practicality the energy deposition values must be scaled up to first wall fluxes anticipated by ITER, which is developed in the next section 3.7. It is anticipated

that pulses in ITER will liberate 2.38×10^{14} n / cm^2 /s for DT campaign (M.R. Gilbert and J.-Ch. Sublet, 2011).

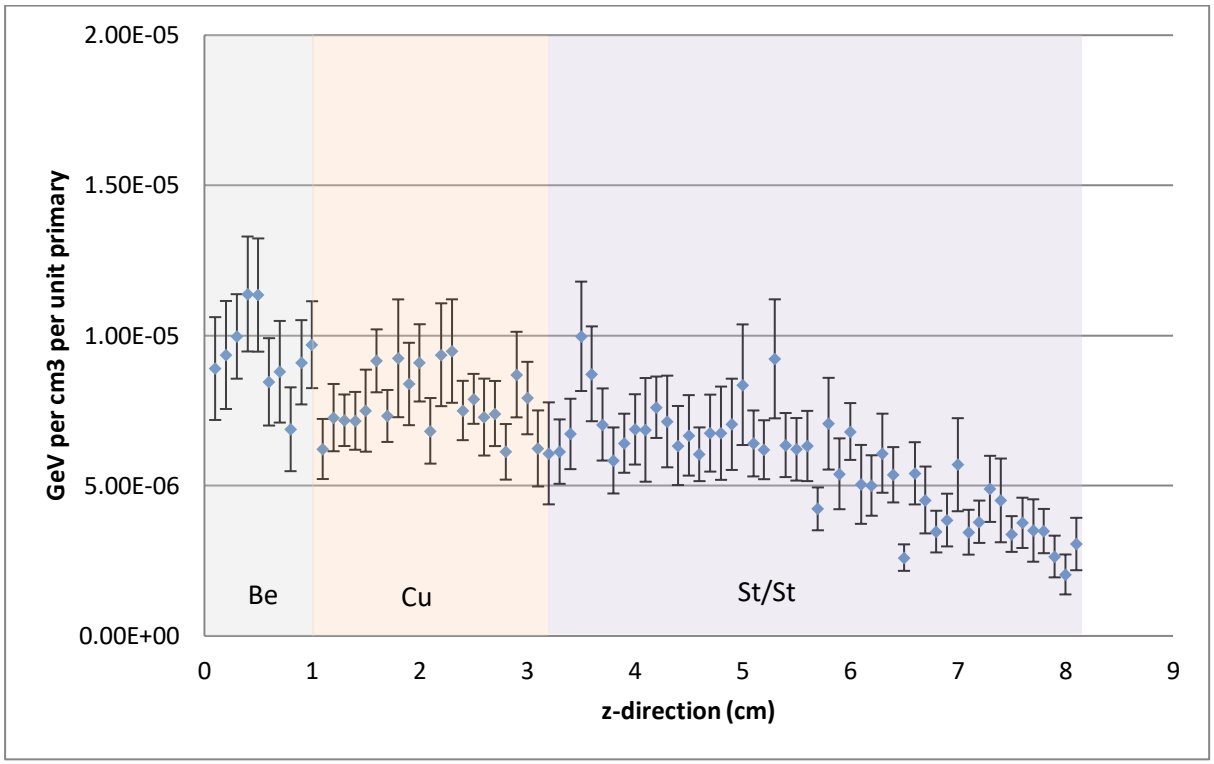

Figure 7: Average energy deposited in section A bins with standard error of mean. Geometry boundaries overlaid as per model in figure 6.

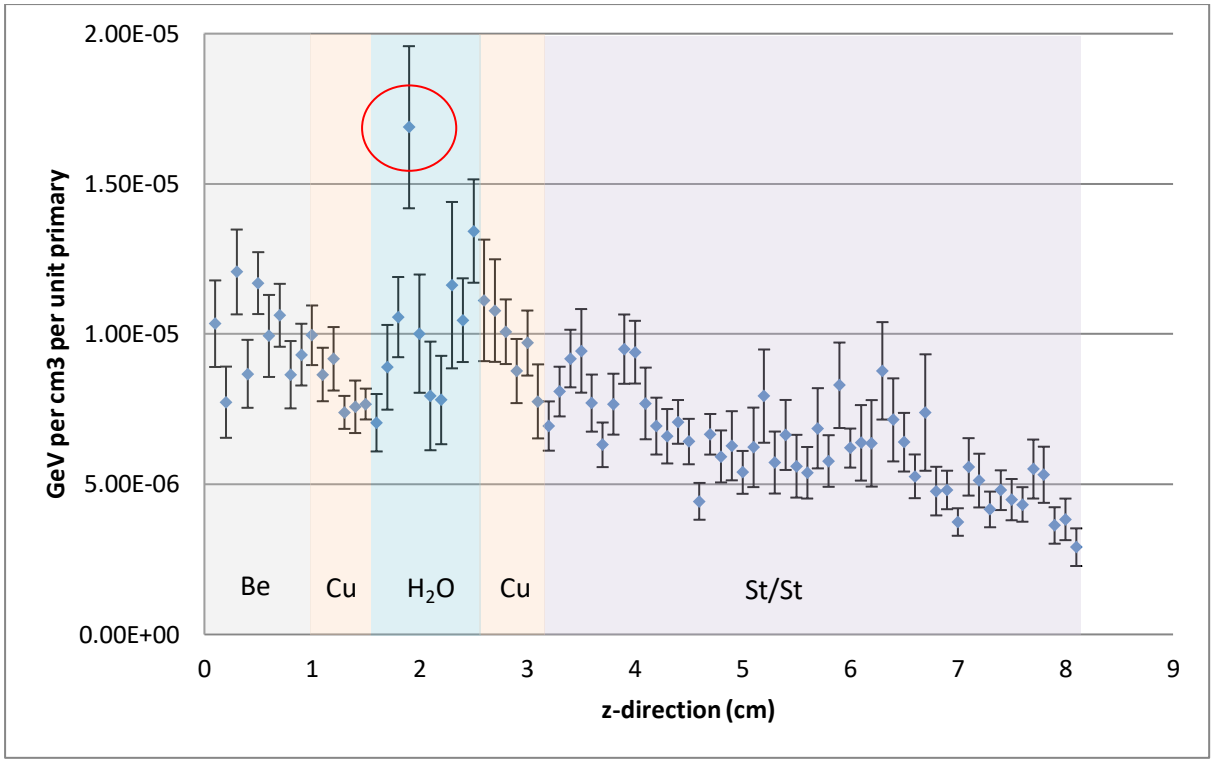

Figure 8: Average energy deposited in section B bins with standard error of mean. Geometry boundaries overlaid as per model in figure 6. Notice large energy deposition marked in red circle, midway through the cooling water channel

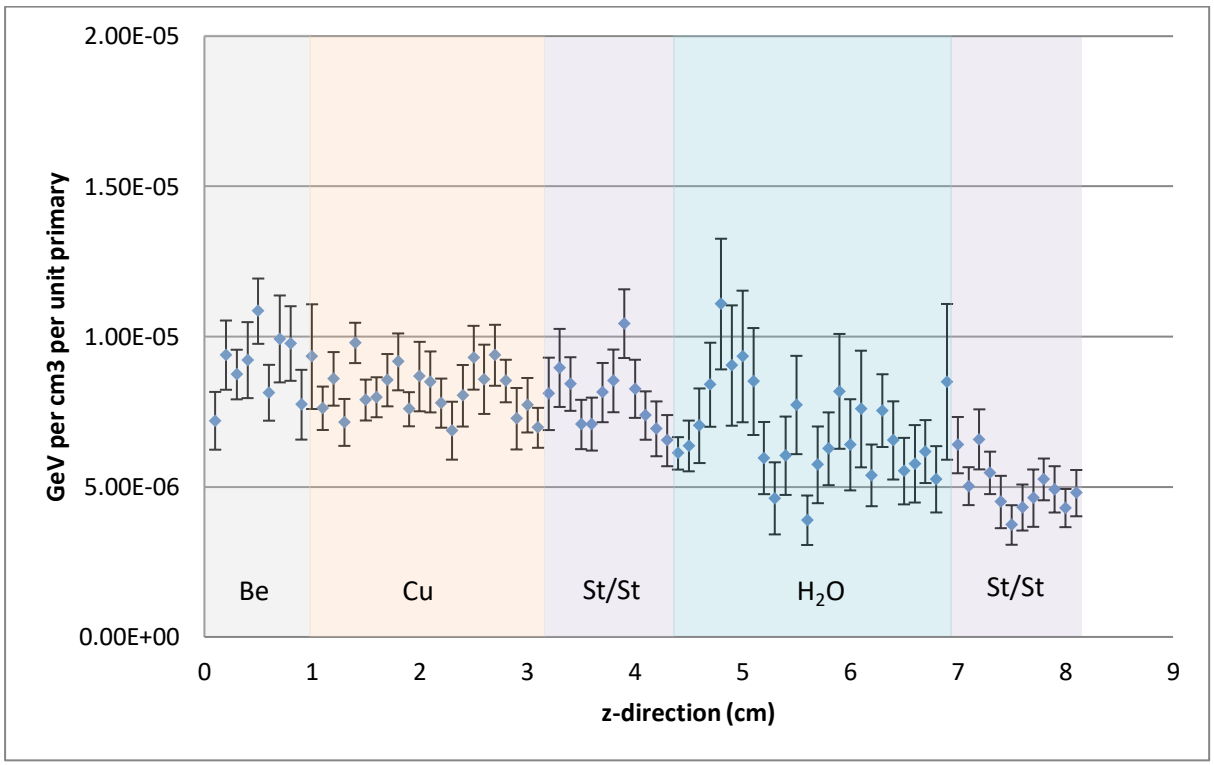

Figure 9: Average energy deposited in section C bins with standard error of mean. Geometry boundaries overlaid as per model in figure 6. Less significant energy deposition in large cooling water channel

3.7 Power calculations to determine theoretical thermal energy output of FW panel model

In the previous section FLUKA gives the energy deposited in GeV/cm^3 for each bin which is 0.1cm thick in the z direction. The actual volumetric sizes of these equal bins are as follows:

	Thickness (cm) [z-direction]	Height (cm) [y-direction]	Width (cm) [x-direction]	Volume (cm^3)
Section A	0.1	0.6	4.8	0.288
Section B	0.1	1.2	4.8	0.576
Section C	0.1	1.2	4.8	0.576

Table 2: Bin sizes for all three sections

The total energy deposition for all 81 bins per a section was calculated as follows:

Section A = 1.08E-02 GeV/cm^3 ; Section B = 1.23E-02 GeV/cm^3 ; Section C = 1.19E-02 GeV/cm^3

Since the energy deposited is per cm^3, the given values had to be reduced proportionally to reflect the actual energy deposited in the section.

Next the values were converted to Joules by multiplication using 1 J = 1.602E-19 eV. Now the values were scaled up by multiplication to the full flux intensity of 2.38E+14 n / cm^2 /s resulting in three heat fluxes for the sections:

	Heat Flux	
	J/cm^2. s	W/cm^2
Section A	1.19E+02	118.70
Section B	2.70E+02	270.27
Section C	2.62E+02	262.05

Table 3: Heat fluxes in sections A, B and C.

Due to the models geometric symmetry as seen in figure 6, the front facing surface area of the model is comprised of total sum of 2 times sections A, 2 times sections B and 1 times section C having areas 2.88cm^2, 5.76cm^2 and 5.76cm^2 respectively. Thus, the total heat flux for each section can be calculated and also the total heat flux for the model made up of these sections. A calculated value of 5306 W of thermal power is generated in the model. Since the model is a small representation of the FW armor measuring 4.8 cm by 4.8 cm = 23.04cm^2, approximately 434 of these models would represent 1 m^2 of the FW armor. Multiplying the model heat flux by 434 will provide a heat flux of 2.3 MW/m^2. This is consistent with ITER normal heat flux panels designed for up to 2 MW/m^2 and enhanced heat flux panels which can handle 4.7 MW/m^2.

3.8 Rate of internal heating

The energy generation from all the nuclear reactions depositing energy to heat the FW panel can be calculated for each section and for each 1mm layer. Noting that sections B and C have twice the volume as section A, this will result in these sections having at least double the heating rate. It can be observed that sections B and C have relatively 2.2 to 2.3 times more heating rate than the outside section A. This is likely due to geometry, particularly because section B and C have water columns whereas section A does not. See figures 10, 11 and 12 of the energy release rate H (W/cm^3) with a 3^{rd} order polynomial fit and the equation describing the function. The polynomial function is used in the heat transfer section of this dissertation in order to accommodate for reverse heat flow, that occurs on the high peaks seen below. Essentially the polynomial function describing the heat flux smoothens out the energy released so that the assumption can be made that heat is travelling from hotter left side to the cooler right side in the z-direction. The assumption implies that the temperature at the FW surface is the highest in all sections, and the temperature on the back wall of the stainless steel layer is the coolest. In the practical design, the coolant channels are to be the coolest always so that the heat energy can be directed at the flowing fluid for convection heat transfer.

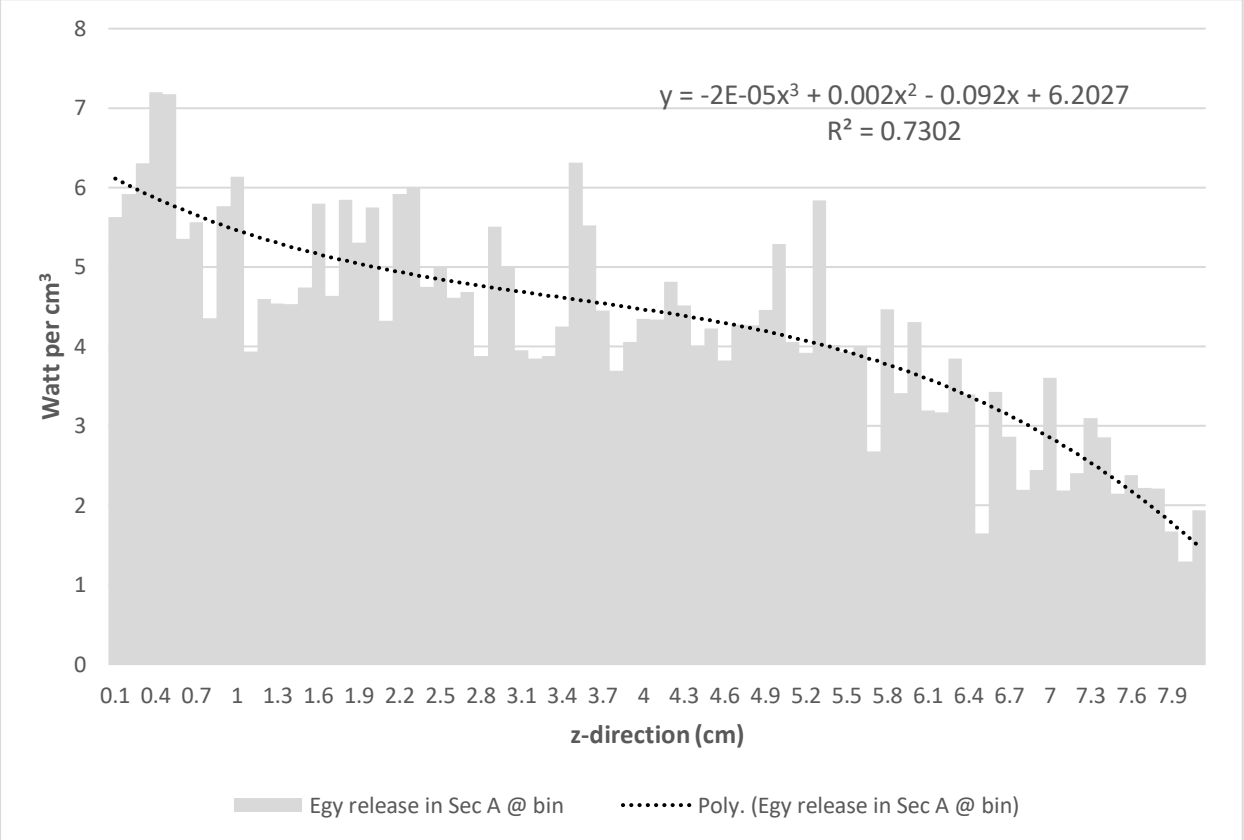

Figure 10: The heat flux or energy release rate (W/cm^3) per bin in Section A

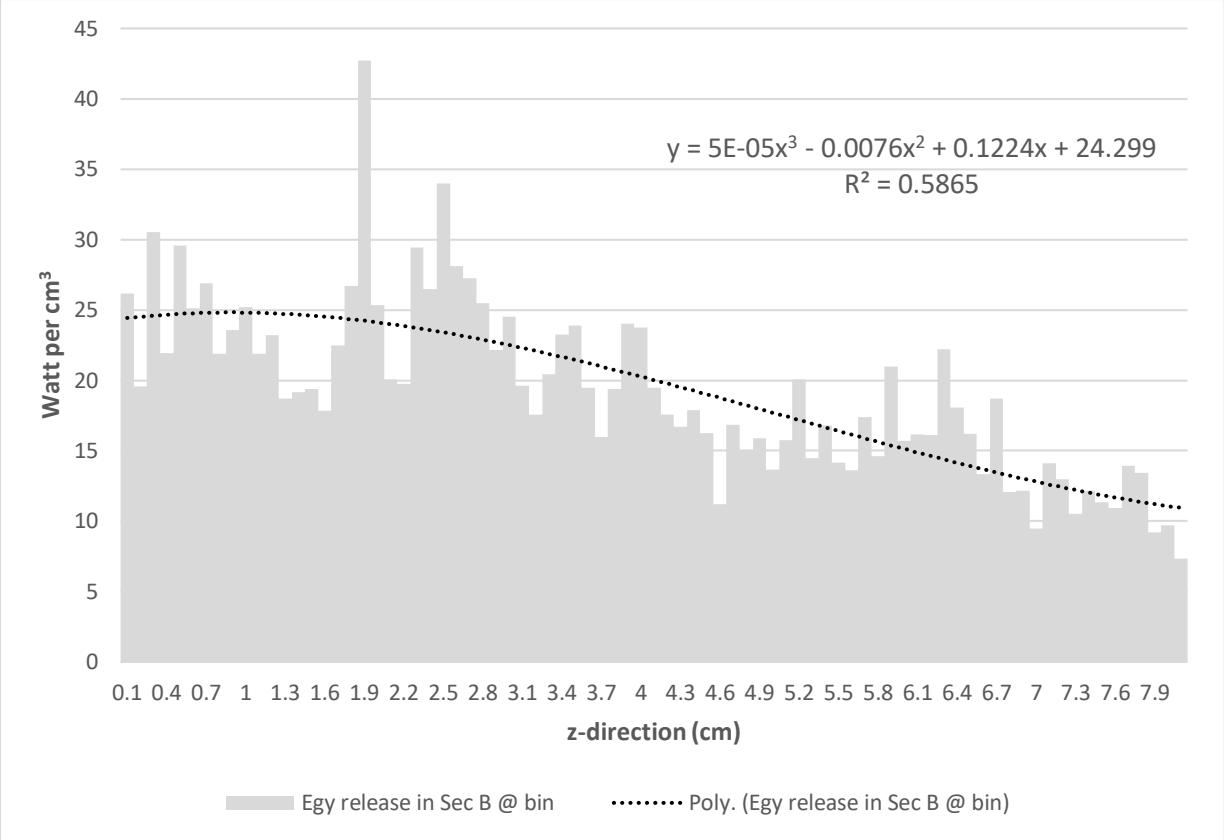

Figure 11: The heat flux or energy release rate (W/cm³) per bin in Section B

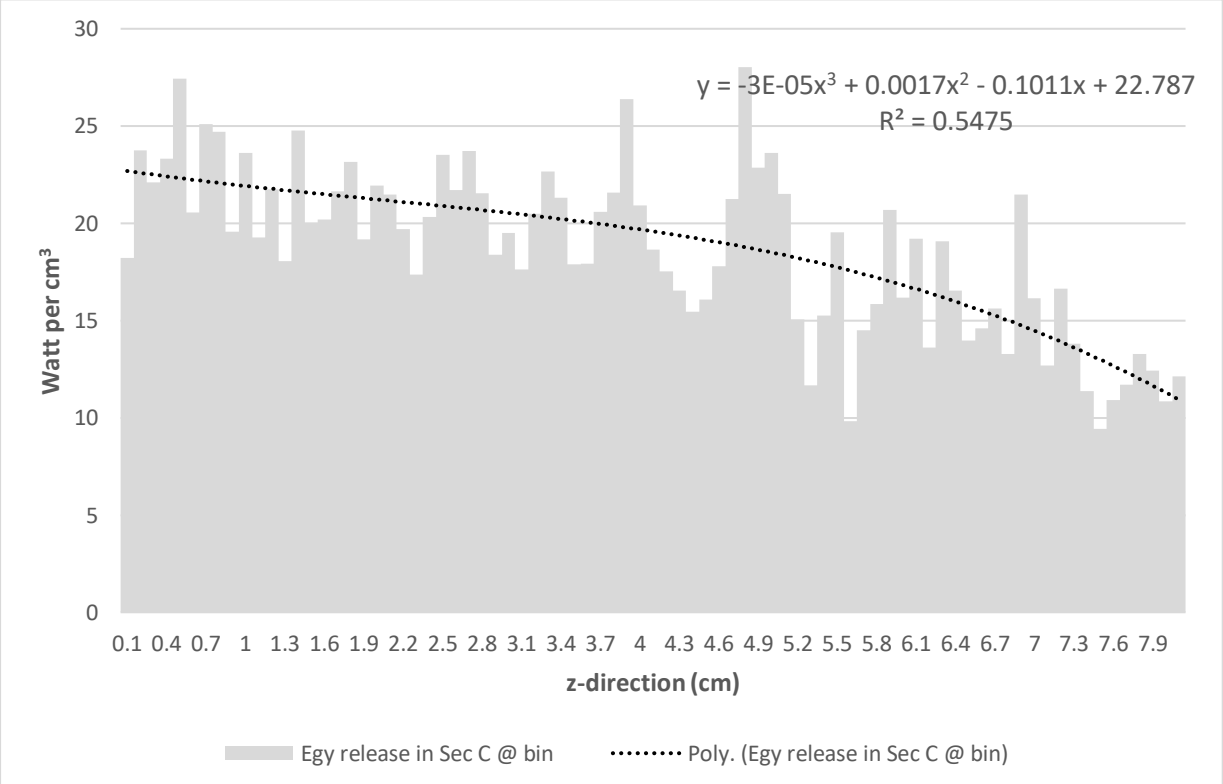

Figure 12: The heat flux or energy release rate (W/cm³) per bin in Section C

4 Plotting the neutron flux

As mentioned, a second scoring was performed on the geometry using USRBIN for neutron particles to provide a neutron flux through the geometry. Again, the same 81 bins of 1mm wide were used over the same three distinct sections A, B and C. This neutron particle scoring was performed in conjunction with the energy deposition scoring. FLUKA scored both neutron particles and energy deposition at the same time.

The requirement for knowing the neutron flux within the FW panel model is not needed for performing the heat transfer calculations in the subsequent chapter, however it is always of great interest to nuclear physicists to know the neutron flux throughout the model. Similar to the energy deposition, FLUKA output 4860 values for the same three sections A, B and C in n/cm^2/s/primary. The flux values were extremely small and represent a fraction of 1 neutron since FLUKA normalized the results. As with the energy deposition, the 20 cycles for neutron particles had to be summed together for each 1 mm wide bin, for each section.

Recalling that the full flux intensity of ITER, DT campaign will be approximately 2.38×10^{14}n/cm^2/s, we are able to scale up the FLUKA output results to have more practical plots of the neutron flux. The following graphs are plotted for each section, indicating the total neutron flux for primary, secondary neutrons etc.

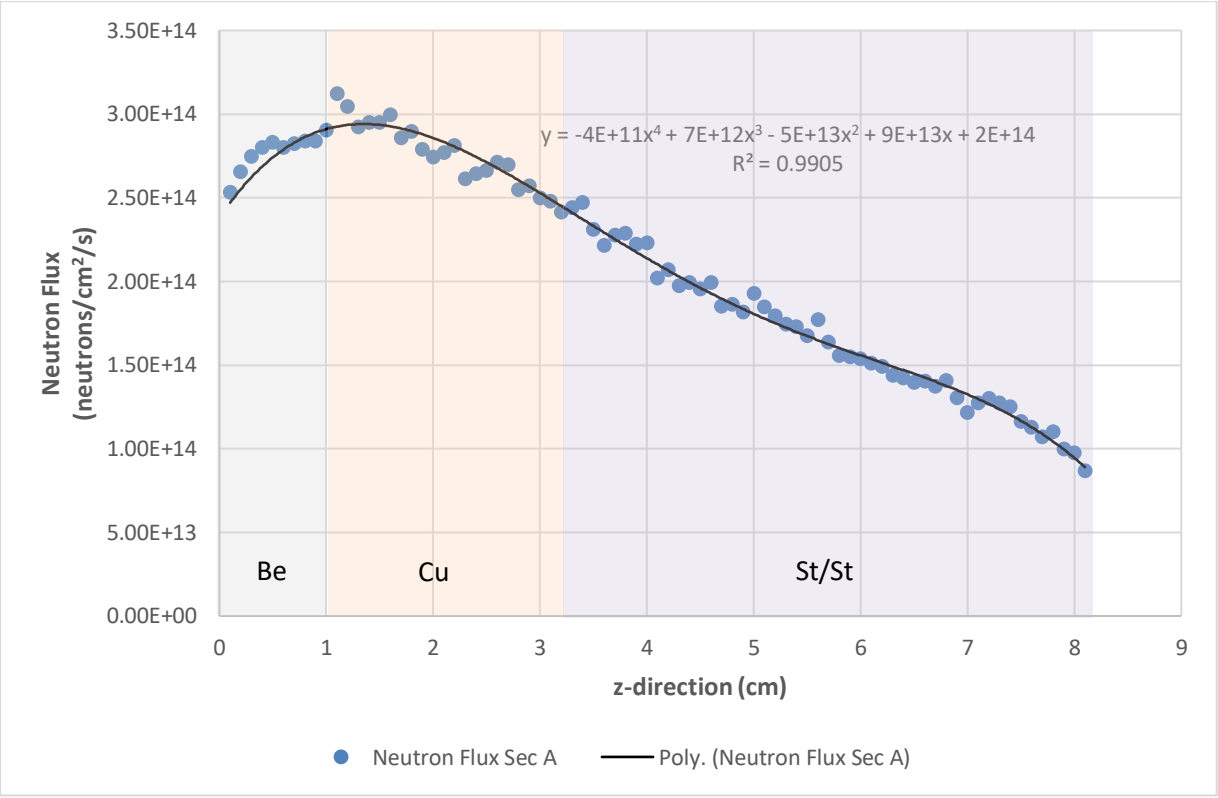

Figure 13: The neutron flux for all neutrons through section A at full flux intensity. Geometry boundaries overlaid as per model in figure 6.

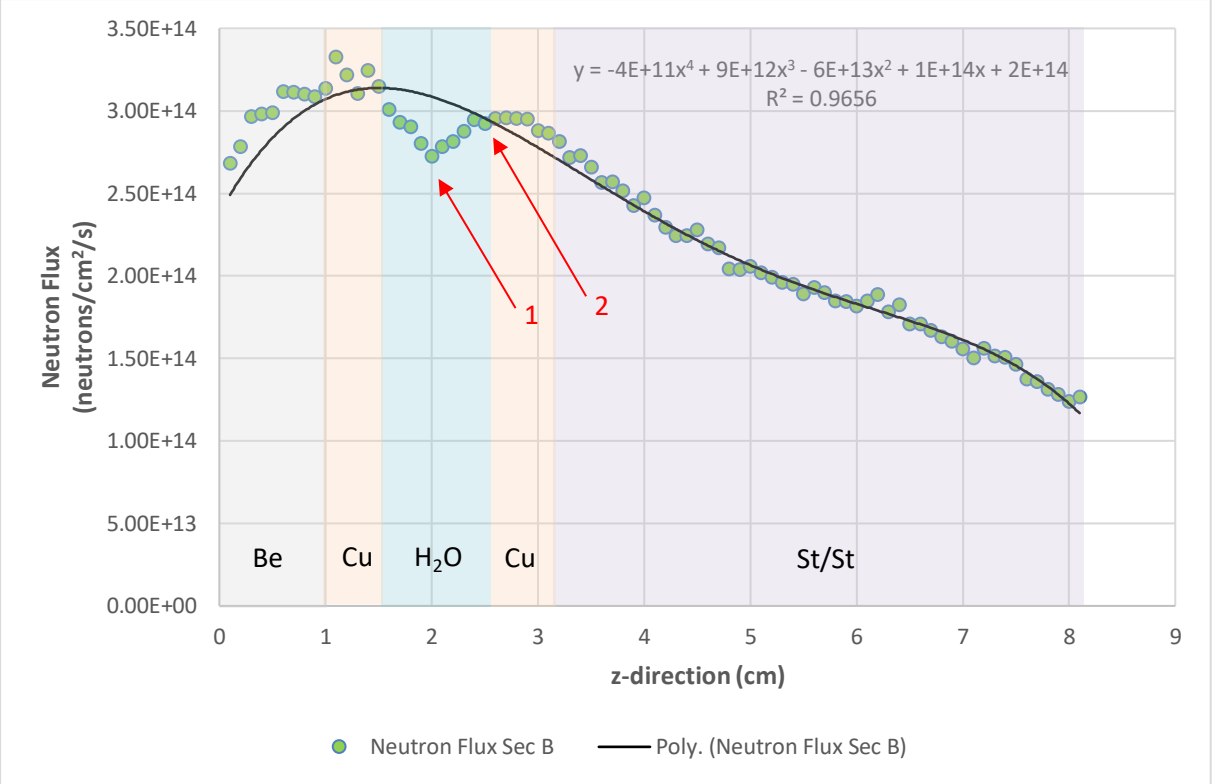

Figure 14: The neutron flux for all neutrons through section B at full flux intensity. Geometry boundaries overlaid as per model in figure 6. Note 1: Observe dip in neutron flux as pass through centre of water channel. Note 2: Observe neutron flux recover once out of water channel possibly due to in-scattering from copper

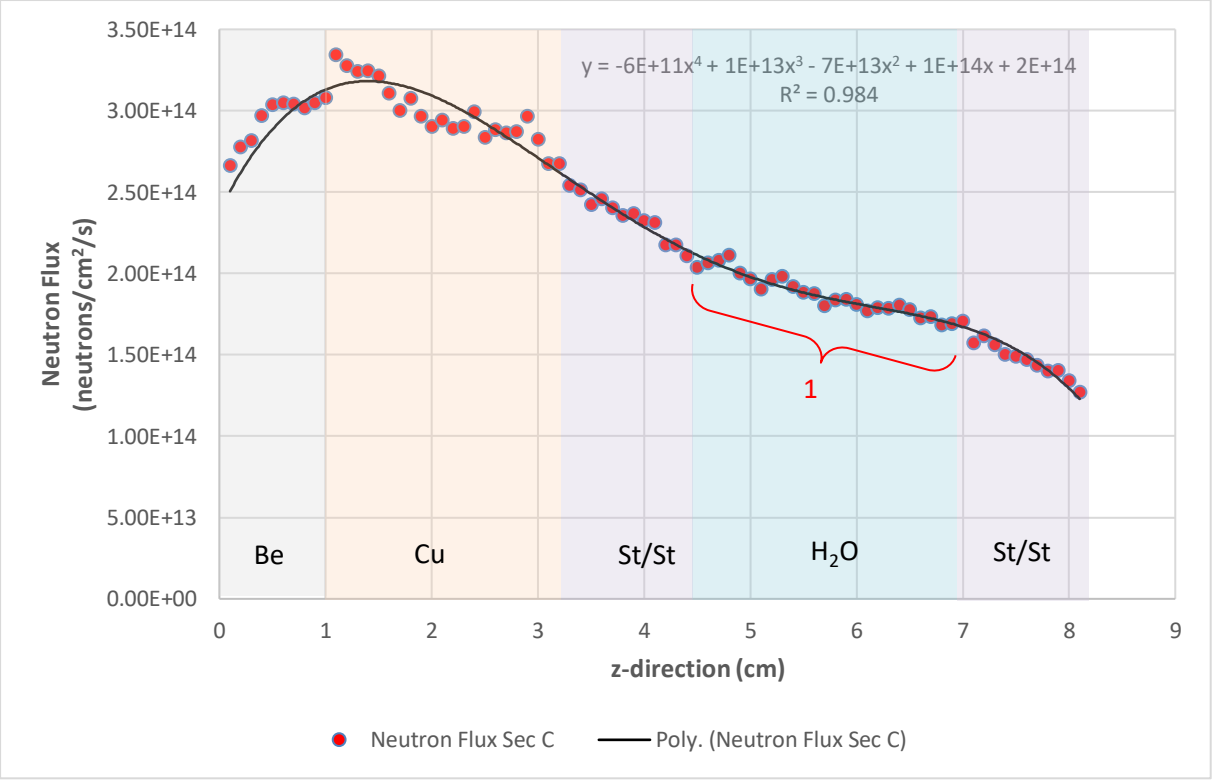

Figure 15: The neutron flux for all neutrons through section C at full flux intensity. Geometry boundaries overlaid as per model in figure 6. Note 1: Large water channel has no noticeable impact on neutron flux, likely due to energy spectrum being different.

A 4^{th} order polynomial trendline is plotted to represent the data. This polynomial trend line is merely a guide to the observe and it does not mean that the neutron flux is following a 4^{th} order trend. The trendlines are forced to intercept at 2.38E+14 for z = 0 cm as this is the initial starting flux. R-squared values of these polynomials are accurate ranging between 96.5 and 99%. As can be seen in all three plots for areas of section A, B and C, the neutron flux actually increases. This can be attributed to the neutron multiplication (chain 3) nuclear reactions of fast neutrons with beryllium. Throughout the 10 mm thick beryllium layer neutron flux increases by as much as 25 to 30%. Beyond the beryllium layer, neutron flux begins to decrease linearly through the copper and stainless steel layers as z increases.

One feature that should be pointed out in figure 14 is the pronounced drop in neutron flux in section B, as the neutrons pass through the water column. It can be observed that neutrons are being absorbed in the water column, showing a decrease in neutron flux. It is theorized that the neutron flux recovers and increases due to in-scattering from the surround copper at z = 25mm. Also recognizing that the bins are rectangular parallelepiped bodies, but the geometry of the water channel is cylindrical we can observe a change in the ratio of water to copper. As the ratio decreases in the bins, we are changing the material which greatly affects the nuclear characteristics.

5 Fission versus Fusion

A noteworthy difference between a conventional PWR and a fusion reactor is that in the PWR, the fission energy, mostly from the fission products is directly absorbed in the fuel rods, causing the fuel rods to increase in temperature. This prompt energy from fission is around 87% of the total energy, and of this, the fission fragments account for over 90%. The fission fragments are easily stopped and travel only a fraction of a millimeter from their point of origin. Below is a table which summarizes how the energy is distributed amongst the various products of fission for U-235.

	Average emitted energy per fission (MeV)
Prompt energy:	
Fission fragments	168
Fission neutrons	5
ɣ emission: (photons and internal-conversion electrons)	7
Radioactivity:	
B decay: (electrons)	8
B decay: (neutrinos)	12
ɣ emission: (photons and internal-conversion electrons)	7
Total	207

Table 4: Distribution of emitted energy on average from a single neutron-induced fission of ^{235}U (Lilley, 2001)

In a PWR, about 13% of the energy is released in radioactive decay. The energy is carried by electrons, gamma rays and internal-conversion electrons. All of this energy is absorbed and converted into heat, however the neutrino energy is not recoverable. The net result is that about 200 MeV per fission is recoverable for use and is generally an accepted value (Lilley, 2001).

In contrast a D-T fusion reactor produces 17.59 MeV of energy per fusion reaction, not even a tenth of the energy as compared to the neutron induced fission of U-235 per reaction. The discrepancy in the energies lies in the number nucleons involved in the reactions – more than 236 nucleons for fission and 5 nucleons for fusion. On a nucleon basis, fusion releases 17.59/5 = 3.52 MeV per nucleon, while fission releases 200/236 = 0.85 MeV per nucleon. So fusion produces over 4 times more energy than fission when making a mass comparison.

As mentioned previously the 3.5 MeV alpha particle in the fusion reaction is absorbed into the plasma and contributes to the internal heating of the plasma. This energy does not contribute to the heating of the blanket. Only the single 14.1 MeV fusion neutron emitted from the plasma starts the series of nuclear reactions, with a very high probability initially that the fusion neutrons gradually lose their energy by successive scatterings within the FW beryllium armor. The elastic scattering is converted to heat which will increase the temperature of the beryllium layer. After many scattering events, the probability for the neutron to be absorbed increases, and at this point a multitude of

nuclear reactions can occur with every neutron interaction yielding, in most cases, an energy deposition within the beryllium in the form of charged particles radiation. The radiation is absorbed locally within the FW beryllium. This description of neutron scattering and neutron absorption resulting in radiation is notably similar to the radioactivity decay heat within the materials of a conventional PWR.

6 Thermodynamic heat transfer through the working model

It can be seen in the MC model, that neutrons are penetrating all layers of beryllium, copper, steel and the water columns in the FW panel model. The intensity of the neutron flux is reduced by 37% in section A, whereas the inner sections B and C both see a reduction of 53%. The 10 mm thick beryllium layer is acting as a moderator as well as a neutron multiplier, recovering the energy from the fusion neutrons. Neutron interactions do occur in the copper, steel and water causing energy to be deposited from neutron scattering and radiation. It can be seen from the model that energy deposition occurs in all layers to various degrees, though the FW beryllium layer is absorbing the most energy and consequently results in the highest temperature in the blanket.

Due to the beryllium layer having the highest temperature, the heat transfer mode is by conduction to the relatively cooler copper layer. A heat transfer rate $\dot{q}$ (W/m^3) is a function of the temperature of the two layers, the layer geometry and the thermal properties of the materials. Since the inside volume of the tokamak fusion reactor is a vacuum, there is no conductive or convection heat transfer in the direction into the vessel except for radiation heat transfer. The transfer of heat via thermal radiation is done by means of photons in electromagnetic waves. As the tokamak reactor is a closed vessel any thermal radiation will be re-absorbed by the FW beryllium layer in an opposing module therefore the radiation losses are negligible.

The ITER blanket module element is a sandwich of beryllium bonded to copper alloy bonded to structural stainless steel. Apart from a thermal radiation from the beryllium layer, the primary heat transfer mode is by conduction from the beryllium to the copper to the stainless steel. The heat energy will flow in the positive z direction in the model. At the copper and stainless steel to water interface, the heat transfer mode will be by convection. Convection heat transfer is the transfer of heat from one place to another by the movement of fluids, a process that is essentially the transfer of heat via mass transfer.

Literature predicts that the operating temperature limit of the beryllium layer will be <600 °C. Beyond 600 °C radiation induced swelling of beryllium occurs which is problematic from a mechanical point of view. Another constraint is that the beryllium oxide surface layer will begin to crack and even spall off at temperatures >700 °C (known as breakaway oxidation). Spalling of this oxide layer will contaminate the reactor vessel. Furthermore, precipitation of helium gas from both grain boundaries and inside the grains begins at 700 °C and peaks at 1200 °C. All the aforementioned

negative affects must be avoided by operating the beryllium layer below 600 °C (Dombrowski, 1996). For the heat transfer to flow from beryllium to the copper alloy, the beryllium FW will be operating at a higher temperature than the copper alloy layer. ITER states that the cooling water system will be suppling water at 70 °C at 4 MPa. This high-pressure water, which has a boiling point of 250.4 °C at 4 MPa, will help with temperature stability and accommodate the pulse operation of the fusion reactor. One can see that ΔT across the length of the blanket module is apparent and a drive for heat transfer to the cooling water will occur.

A very important material choice was made for the second layer of the blanket. The second layer is to act as a heat sink, taking conductive heat transfer from the FW beryllium armor. The main requirements for the layer is a high thermal and electrical conductivity. ITER has proposed to use a Cu-Cr-Zr alloy due to a combination of high strength and high thermal and electrical conductivity when compared against other copper-based alloys (A.A. Suvorova, 2018). Copper has the second best thermal conductivity around k = 401 $W.m^{-1}.K^{-1}$ at STD 20 deg C, and is only surpassed by the very costly silver which has slightly higher thermal conductivity around k = 429 $W.m^{-1}.K^{-1}$ at STD 20 deg C. From an economical point of view, copper is by far a more cost effective material and is much more readily available.

The thermal conductivity *k* of materials of the ITER blanket module can be seen in the following table 5. Due to copper's much higher thermal conductivity versus beryllium, conductive heat transfer readily moves the heat from the beryllium allowing any small temperature variations in the beryllium to be rapidly minimized. The table also demonstrates that thermal conductivity decreases with an increase in temperature. This property of the metals negatively retards heat transfer, causing higher temperatures to be experienced in the FW panel.

Element/Material	Thermal conductivity, *k*	
	(W/m. K @ STD 20 °C)	(W/m. K @ 200 °C)
Beryllium	200	130
Copper	401	300
Stainless Steel	19	16
Water	0.6	0.654 at 4 MPa

Table 5: Thermal conductivity of materials in the FW panel

6.1 Heat diffusion equation

The general heat diffusion equation is a partial differential equation, describing the distribution of heat (or variation in temperature) in a particular body, over time. In a cartesian coordinate system, the equation can be described as follows:

$$\frac{\partial^2 T}{\partial x^2} + \frac{\partial^2 T}{\partial y^2} + \frac{\partial^2 T}{\partial z^2} + \frac{\dot{q}}{k} = \frac{\rho c_p}{k}\frac{\partial T}{\partial t}$$

Where the terms and constants are defined as:

$\frac{\partial^2 T}{\partial x^2}$; $\frac{\partial^2 T}{\partial y^2}$; $\frac{\partial^2 T}{\partial z^2}$ are the double partial differential change in temperature (variation in temperature) divided by the change in the x, y and z directions respectively.

$\frac{\partial T}{\partial t}$ is the change in temperature over change in time.

$\frac{\dot{q}}{k}$ is the rate of heat generated (release or absorbed) per unit volume divided by that materials conductivity.

$\frac{\rho c_P}{k}$ is the density of the material multiplied by the specific heat of the material divided by the thermal conductivity of the material.

T is the temperature of material (K)

x, y and z are the dimensional lengths in the x, y and z directions respectively (m)

t is for time (s)

k is the materials conductivity (W/m. K)

$\dot{q}$ is the rate at which heat is generated per unit volume of the medium (W/m^3)

ρ is the density (kg/m^3)

c_p is the specific heat capacity (J/kg. K)

From the solution of the heat diffusion equation, we can obtain the temperature field as a function of time. We will analyze the model in 1-d because the model has very large dimensions in the x and y direction when compared to the values of the model in the z-direction. Consequently, the partial derivatives with respect to x and y will tend towards zero. Therefore, we can simplify the heat diffusion equation as $\frac{\partial^2 T}{\partial x^2}$ and $\frac{\partial^2 T}{\partial y^2}$ both become zero. Additionally, the model is to be analyzed whilst in a steady state, therefore the temperature will not be changing as a function of time. Thus, the partial derivative with respect to time, $\frac{\partial T}{\partial t}$ is zero.

As we are only dealing with 1 dimension, the equation reduces to the ordinary differential equation:

$$\frac{d^2 T}{dz^2} = -\frac{\dot{q}}{k}$$

The objective is to be able to calculate the temperature with respect to the depth, z. In order to do this, we will need to integrate this function twice, as T(x) is a second derivative.

$$\frac{dT}{dz} = -\frac{\dot{q}}{k}z + c_1$$

$$T = -\frac{\dot{q}z^2}{2k} + c_1 z + c_2$$

To solve for c_1 and c_2 we will apply boundary conditions specifically for the model. Below is a simplified diagram of the FW panel with internal nuclear heating. As mentioned, the front face of the beryllium layer is in a vacuum meaning that heat transfer to the vacuum is zero.

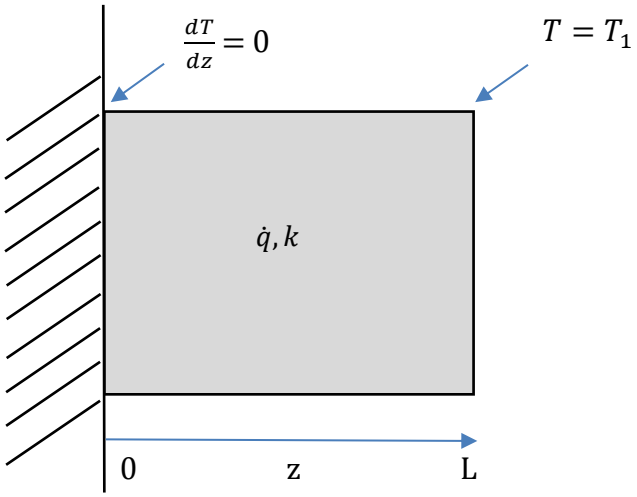

One of the boundary conditions is:

$$\left.\frac{dT}{dz}\right|_{z=0} = 0 \; ; \; c_1 = 0$$

This boundary condition applies at the beryllium and vacuum interface where no heat transfer is to occur due to the vacuum's inability to conduct heat. This boundary is near perfect insulation at z = 0.

The second boundary condition is:

$$T(z = L) = T_1 \; ; \; c_2 = T_1 + \frac{\dot{q}L^2}{2k}$$

This boundary condition applies at the opposite side of the model where z = L. The heat diffusion equation demands that a single reference point temperature is given for a solution, therefore the most convenient reference temperature is T_1 at z = L as this is the most accessible position to take a temperature reading. If one is able to measure T_1on the back of the FW panel, the temperature distribution can be calculated.

Putting the boundary equations back into the second derivative equation gives us the following equation which describes the temperature distribution in the model:

$$T(z) = \frac{\dot{q}}{2k}(L^2 - z^2) + T_1$$

Using this equation we can calculate the temperature distribution of a simple model which has an average energy heat release $\dot{q}$ and average thermal conductivity k, in the z- direction, given by table 6. The energy heat release $\dot{q}$ is sourced from the internal heating values from the figures 10, 11 and 12.

	Section A	Section B	Section C
Average:			
Heat release, $\dot{q}$ (W/cm^3)	4.22	19.21	18.63
Thermal conductivity, k (W/cm.K)	0.142	0.088	0.138

Table 6: Heat release and thermal conductivity of sections A, B and C based on model figure 6.

The following graph, figure 16, can be plotted when T_1 = 100 °C and for L = 8.1 cm as per the full depth of the model give in figure 6. Unfortunately we have to force T_1 = 100 °C as a reference point temperature but this does allow us to convienently compare the temperate profile in each section against each other. These temperature distributions are for the central mid-plane for each section. Thermal conductivity plays a very important role in the temperature profiles of the sections A, B and C and as a result section B exhibits a higher delta temperature over the depth of the model due to having the lowest average thermal conductivity. From the graph, figure 16, it can be interpreted that the central section B is the hottest and the outer sections A are relatively cooler.

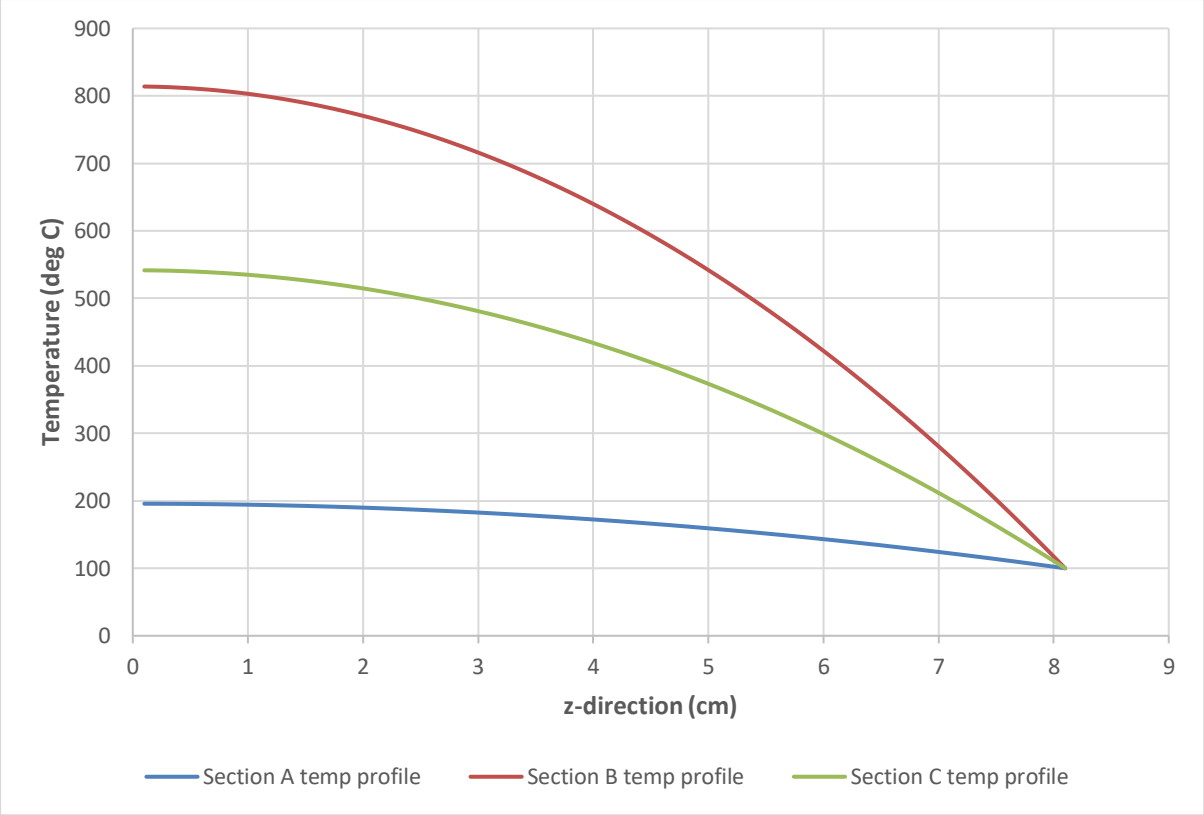

Figure 16: Temperature profile for sections A, B and C using simple model, based on the model figure 6.

There are short comings in using the average energy heat release $\dot{q}$ and the average thermal conductivity k in depicting the temperature profiles of section A, B and C. The calculations are based on a homogeneous material and a constant energy heat release throughout. This is clearly not the case in reality where the sections are made up different materials as in table 5 and with varying heat flux or energy release rates seen in figures 10, 11 and 12. Therefore figure 16 is a generalized representation showing the beryllium FW panel is the hottest and that the temperature decreases to the rear face.

Performing the calculations again using the same equation, we divide the section into the materials that comprise the total section. This is done for each material and its average energy heat release $\dot{q}$, thermal conductivity k as per table 5, over its length in the z-direction. Due to stainless steel having coincidently 50% of the internal heating and a relatively poor thermal conductivity k when compared to copper and beryllium, a large temperature diffential can be observed across the stainless steel section, see figure 17.

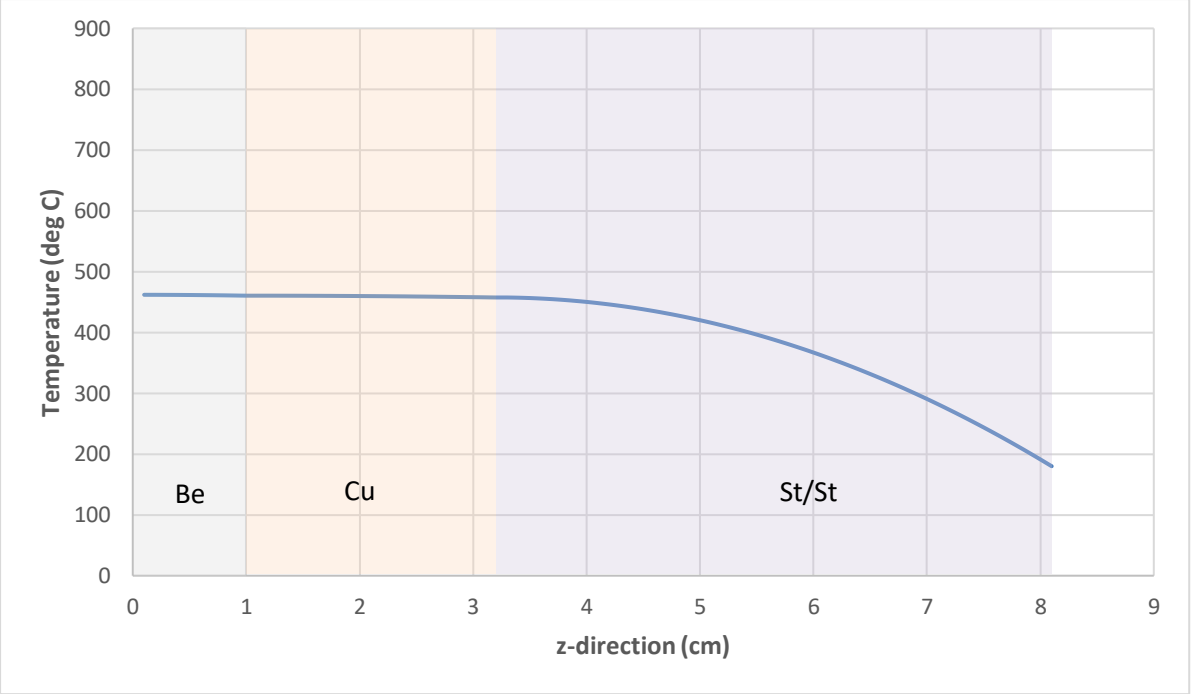

Figure 17: Temperature profile for section A using multiple material model, based on the model figure 6.

Further heat transfer temperature profiles can be computed for sections B and C, however due to the limitations of the heat diffusion equation being calculated in 1-dimension the results are very misleading. This is a short coming of not performing 3-dimensional heat transfer. Engineers will generally use a finite element heat transfer (FEHT) software to do these 3-dimensional calculations, however this is beyond the scope of this dissertation.

One obvious short coming for example, as seen in figure 18, is that the very high temperatures reached in the stainless steel in section B would be lower in reality since the heat energy would rapidly travel in the y-direction to the large coolant pipe. This would make a very strong depression in the temperatures seen in the stainless steel in section B.

The graph of section B and C show typical parabolic shaped temperature profiles at the coolant pipes in the model. The dominant mode of heat transfer is by convection in the coolant pipes, which is also determined to be a turbulent flow in both pipes in the following section. The turbulent flow in the coolant pipes greatly enhances heat transfer to the coolant water since the velocity of flow fluctuates and has a highly disordered motion. This high velocity fluctuations and disorder is responsible for high heat transfer rate and resulting heat transfer coefficient. A surface temperature for all coolant pipes has been selected to be approximately 180 °C, in order that a sufficient delta temperature can be present between the pipe walls and the coolant fluid of 70 °C at 4 MPa.

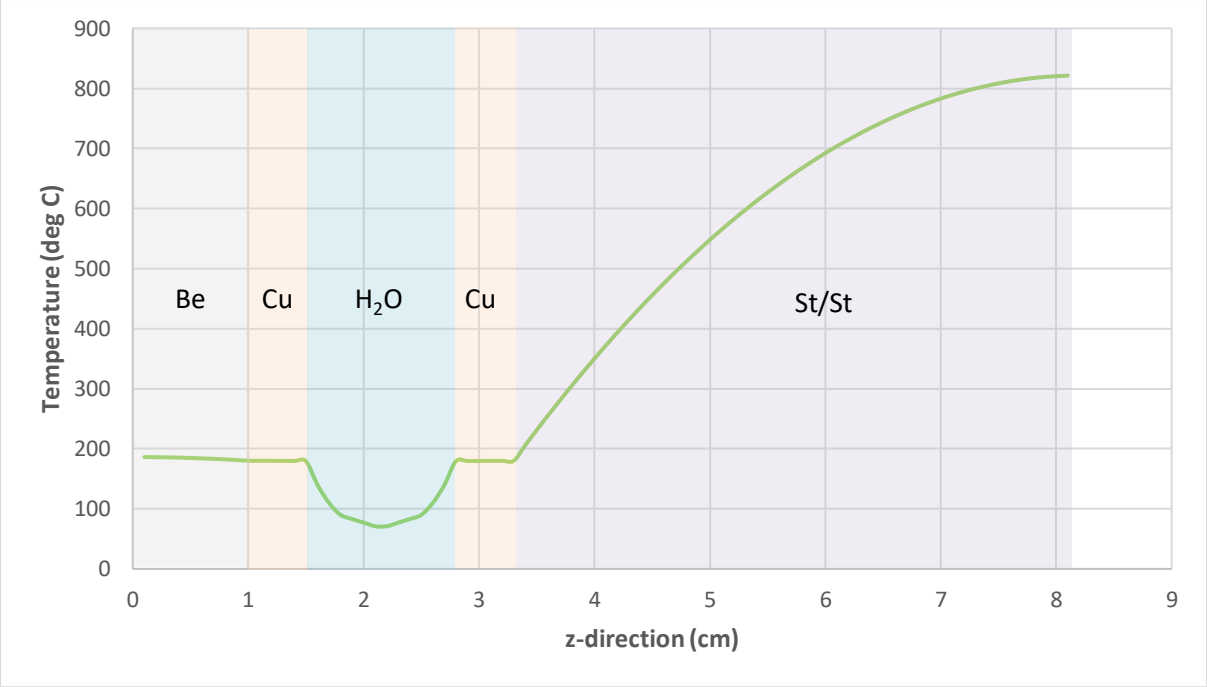

Figure 18: Temperature profile for section B using multiple material model, based on the model figure 6.

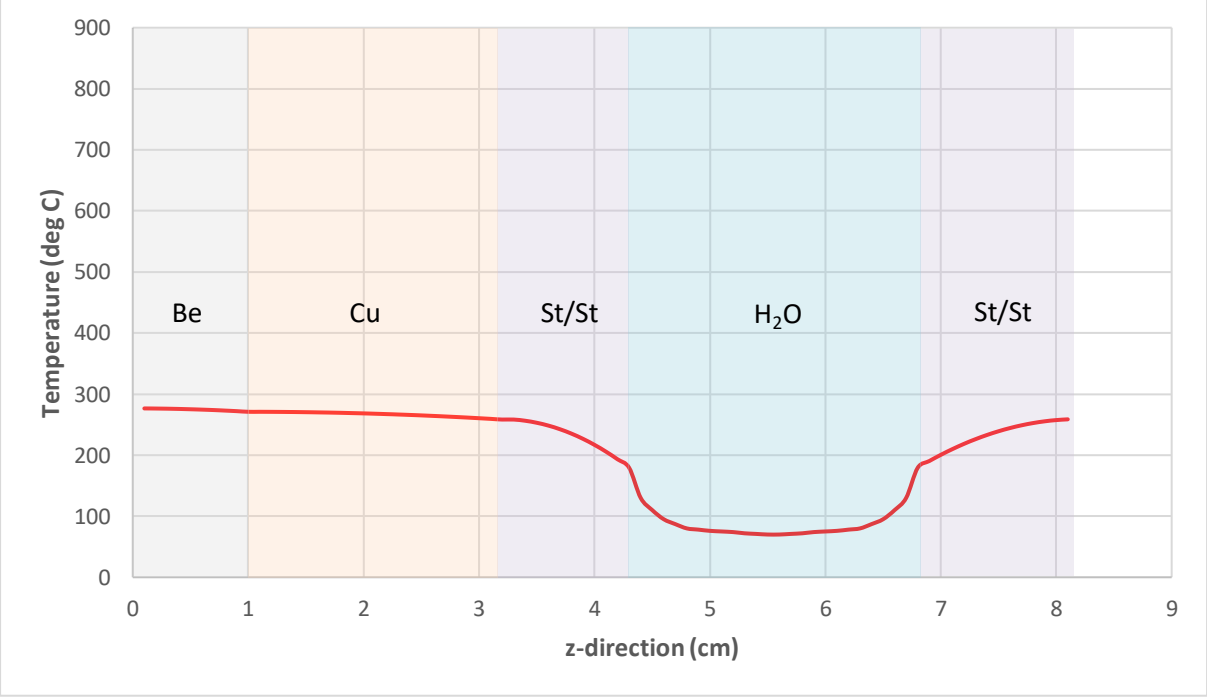

Figure 19: Temperature profile for section C using multiple material model, based on the model figure 6.

6.2 Heat transfer to cooling fluid

The nuclear heating in the FW panel model was calculated, however all this heat energy must be transferred to the cooling fluid, under steady state conditions. In the fusion reactor to operate in a steady state, all the heat produced must be removed as fast as it is produced. Heat transfer from the FW panel must be greater than the heat generation rate otherwise overheating will occur and possible damage to the FW panel. It cannot be underestimated the importance of the design and operation of the coolant system (Heat Generation, 2019).

The heat transferred by conduction through the FW panel is removed by convection through the coolant channels. The law governing this process is Newton's law of cooling:

$$q = hA(T_s - T_\infty) \quad (1)$$

where q is the convection heat rate, h is the coefficient of heat transfer (W/m^2.K), A is the surface area of the pipes (m^2), T_s and T_∞ are the temperatures (°K) at the surface of the pipe and inside the coolant respectively. The equation appears deceptively simple however determining the coefficient of heat transfer *h*, is complex and a numerical solution is used as follows with several assumptions.

Firstly, referring to ITER literature, ITER is assumed to have approximately 600 m^2 of blanket modules (BM) and a mass flow rate, $\dot{m}$ of 3140 kg/s of cooling water at 70 °C at 4 MPa running through the coolant channels (Iter Website, 2019). An assumption is made that the flow of coolant is evenly distributed over the entire blanket, therefore the average mass flow rate is 5.23 kg/s (per m^2 of blanket). This is equivalent to a volume of water of 0.00523 m^3/s by using the generally accepted assumption that liquid water is incompressible.

With this the mean velocity of coolant can be calculated (per m^2 of blanket) as follows:

$$v = \frac{V}{A} \quad (2)$$

To calculate the pipe surface area A, all the areas of the small cooling pipes and large cooling pipes must be the summed together for a 1 m^2 blanket. As the model evaluated in this dissertation is 4.8 cm high (y-direction), a total of 20.83 of these models will fit in a meter. Thus, the area of all the pipes is 0.014137 m^2 and the mean velocity of the coolant is calculated to be 0.37 m/s. Table 7 over page summarizes the calculations.

ITER characteristics:		Units		Comment:
Mass flow rate	3140	kg/s		
Blanket surfaces area	600	m^2		
Model characteristics:				
Diameter of small pipe (D)	0.012	m		
Diameter of large pipe (D)	0.024	m		
Height of model	0.048	m		
Kinematic viscosity (***v***)	4.12E-07	m^2/s		
Thermal diffusivity (α)	1.47E-07	m^2/s		
Thermal conductivity of fluid (k)	0.6	W/m.K		Water at 70 °C
Specific heat capacity of fluid (C_p)	4179.6	J/kg·K		Water at 70 °C
Density of fluid (ρ)	977.81	kg/m3		Water at 70 °C and 4 MPa
Temperature at surface of all pipes (T_s)	180	°C		Assume all pipes same temperature
Temperature of bulk fluid (T_∞)	70	°C		Assume all fluid same temperature
Calculations:				
Average mass flow rate ($\dot{m}$)	5.233333	kg/s	per m^2	Assume even distribution of flow
Average volume flow rate (V)	0.005233	m^3/s		Assume in compressible liquid
Models per running meter	20.83333	units		
Area of pipes in 1 model	0.000679	m^2		Two small pipes and 1 large pipe
Area of all pipes for running meter	0.014137	m^2		
Mean velocity of all fluid through 1 m^2 panel	0.370183	m/s		Assume even distribution of flow
Surface area of pipes for running meter	0.037699	m^2	small pipe	
	0.075398	m^2	large pipe	
Calculations of units:				
Reynolds numbers (Re_D)	10792.5		small pipe	Turbulent flow
	21584.99		large pipe	Turbulent flow
Prandtl number	2.803582			
Nusselt numbers	58.52086		small pipe	
	101.8907		large pipe	
Convection coefficient of heat transfer (h)	12134.01	W/m	small pipe	
	21126.54	W/m	large pipe	
Calculation result:				
Total convection heat rate (q)	505583.9	W/m^2	small pipes	
	440136.3	W/m^2	large pipe	
Sum of total convection heat rate (q)	0.945	MW/m^2	All pipes	

Table 7: Convection heat transfer calculations for a 1m² ITER FW panel, based on the model figure 6.

Having calculated the mean velocity of fluid through a 1 m^2 blanket for the small pipe and the large pipe we can proceed to calculate the Reynolds number. The Reynolds number is an important criterion used to predict laminar and turbulent flow regimes. For flow in a pipe or tube, the Reynolds number is generally defined as:

$$Re_D = \frac{Dv}{\boldsymbol{v}} \tag{3}$$

Where D is the diameter of the pipe (m), v is the mean velocity of the fluid (m/s) and $\boldsymbol{v}$ is the kinematic viscosity (m^2/s) of the fluid. The Reynolds number is able to describe the fluid flow as the following:

Re_D < 2300 as laminar flow and, Re_D > 2300 as turbulent flow.

The kinematic viscosity is a measure of a fluid's internal resistance to flow under gravitational forces and this varies with temperature. For water at 70 °C the kinematic viscosity is 4.116E-07 m^2/s.

The Reynolds numbers can now be calculated for the 12mm pipe and the 24mm pipe as the following. Small pipe Re_D = 10792 and large pipe Re_D = 21584. Therefore, both pipes are in a turbulent flow regime as expected. This establishes that the model is describing a system of forced convection heat transfer with turbulent flow.

The convection coefficient of heat transfer *h*, can be obtained for fluids in both pipe as follows:

$$h = \frac{N_U k}{D} \tag{4}$$

Where k is the thermal conductivity of the fluid (W/m.K) and D is the diameter of the pipe (m). The Nusselt number N_U, is the ratio of convective to conductive heat transfer across a boundary and depends on type of flow, geometry and the surface conditions of the pipe. For fully developed (hydrodynamically and thermally) turbulent flow in a smooth circular tube, the local Nusselt number may be obtained from the well-known Dittus-Boelter equation:

$$N_U = 0.023\, {Re_D}^{0.8}\, Pr^n \tag{5}$$

experimentally valid when: 0.6 ≤ Pr ≤ 160,

Re_D ≥ 10000, and

$\frac{L}{D}$ ≥ 10

where *n* = 0.4 for fluid heating, which is applicable to our case; and *n* = 0.3 for cooling. The Prandtl number, Pr, is defined as:

$$\mathrm{Pr} = \frac{\boldsymbol{v}}{\alpha} \tag{6}$$

where **ν** is the kinematic viscosity (m^2/s) and α is the thermal diffusivity (m^2/s). The thermal diffusivity is the thermal conductivity divided by density and specific heat capacity at constant pressure.

For water thermal diffusivity can be calculated as using the equation:

$$\alpha = \frac{k}{\rho C_P} \tag{7}$$

For water at 70°C and 4 MPa, the density ρ is 977.81 kg/m^3, the thermal conductivity k is 0.6 W/m.K and the specific heat capacity C_P is 4179.6 J/kg.K. This results in a thermal diffusivity α of 1.468E-07 m^2/s for equation (7). The calculated thermal diffusivity is inputted into equation (6) to obtain the Prandtl number of 2.803. The calculated Prandtl number is used in equation (5) to obtain the following Nusselt numbers may be calculated for the small pipe and the large pipe:

$N_U = 58.52$ (small pipe); $N_U = 101.89$ (large pipe)

The convection coefficient of heat transfer h, can be calculated for each pipe from equation (4):

$h = 2926.04$ $W/m^2.K$ (small pipe); $h = 2547.26$ $W/m^2.K$ (large pipe)

With convection coefficient of heat transfer calculated the convection heat rate can be calculated using Newton's Law of Cooling (1) and using a T_s of 180°C and a T_∞ of 70°C. A greater delta T will result in a greater convection heat rate. The convection heat rate q, for all the small pipes and all the large pipe per m^2 is:

q = 505583 W/m^2 (all small pipes); q = 440136 W/m^2 (all large pipes)

It is observed that the two smaller pipes have a greater contribution to the total convection heat rate than the single larger pipe. The sum of convection heat rate from all the pipes per m^2 is 0.94 MW/m^2 for the particular temperatures chosen and this specific geometry and operating conditions. This calculation was purposefully calculated based on 1 m^2 of the FW panel so that a comparison between the nuclear heating rate of 2.3MW/m^2 and the convection cooling rate of 0.94 MW/m^2 can be compared. The heating rate is greater therefore the FW panel will increase in temperature beyond the 180°C however as the temperature increases so will the convection cooling rate. An equilibrium will be reached in this case when the temperature reaches 338°C if all parameters remain the same (A. A. Badawi, 2004).

7 Discussion and Conclusions

The internal nuclear heating generated as a result of an incredibly complex system of nuclear interactions do deposit energies locally within the FW panel. The net effect of all the Q-values from nuclear reactions provide a positive energy deposition in the FW panel. This energy deposition is observed to decrease gradually as the depth increases in the z- direction of the FW panel cause the heating up of the FW panel. We are also able to see that the energy deposition also varies in the y-direction due to performing the heat flux for different sections, namely section A, B and C.

The MC simulation performed in this dissertation was only tracking 20,000 neutrons which is but a representation of the real world neutron flux of 2.38×10^{14} n/cm^2/s expected at ITER. The fact that this very small representation had to be scaled up by some factor of 10^{12} in order to reach these very high neutron fluxes, to be able to obtain the real world energy deposition levels, can lend to a magnified error. Fortunately, by using a polynomial fit, for the heat flux in the sections evaluated we are able to eliminate outliers and get a good representation of the actual heat flux or energy release rate in the sections. In performing the theoretical thermal power calculations for our model we were able to determine that the model would be able to produce a heat flux of 2.3 MW/m^2 under the neutron flux of 2.38×10^{14} n/cm^2/s. This theoretical value for the heat flux was consistent with ITER's predictions for normal heat flux panels designed for up to 2 MW/m^2 and enhanced heat flux panels which can handle 4.7 MW/m^2.

Beryllium as a neutron source and neutron multiplier was observed by the plotting the neutron flux for each section A, B and C from the output of the MC simulation. Nuclear reaction channels with beryllium show that 2 neutrons are released when a neutron interacts with beryllium, and 1 neutron is released when a gamma, proton or alpha particle of sufficient energy interacts with beryllium. Figures 13, 14 and 15 depict a marked increase in neutron flux in the 10 mm thick beryllium fusion facing layer. The neutron flux increases by as much as 25 to 30% at the beryllium – copper interface against the initial starting flux, then the neutron flux begins to decrease linearly through the copper and stainless steel layers as z increases. We are also able to observe a noticeable dip in the neutron flux at the first water coolant channel due to neutrons being absorbed by the water. Beryllium is also compared against other solid neutron moderators and is found to be excellent due its low atomic weight. Beryllium has a relatively large elastic scattering cross section for neutrons which helps immensely to extract the energy from the 14.1 MeV fusion neutrons ejected from the plasma.

Linking the internal nuclear heating generated in the FW panel model to plot the temperature profiles within each section of the model we used heat transfer by conduction and convection. Modeling heat transfer is equally complex as the nuclear physics. Whereas a MC simulation was used to model the nuclear interactions, the heat transfer was done without software but by hand calculations. The heat diffusion equation in 1-dimensions was used to approximate the temperature developed internally along a central midpoint in each section throughout the different material

layers of the model. A number of assumptions were made however for heat to move to the coolant channels there must be a sufficient delta temperature across the coolant pipe surface and the bulk fluid temperature. This delta temperature was clearly seen in figures 17, 18 and 19, demonstrating that the model under a high neutron flux ($2.38x10^{14}$ $n/cm^2/s$) is able to provide suitably high temperatures for heating the cooling water system.

A numerical solution for the cooling capacity from the coolant pipes modelled in figure 6 was calculated using Newton's Law of cooling. A convection heat transfer calculation for a 1 square meter of FW panel was performed and compared against the theoretical heat flux generated from the internal nuclear heating. It was shown that fluid flow in the coolant channels will be turbulent since Reynolds number was greater than 10,000. Turbulent fluid flow will increase heat transfer to the coolant, which is highly beneficial and was certainly designed with this purpose in mind. Using a coolant temperature of 70 °C at 4 MPa and a surface temperature of the coolant pipes of 180°C, we are able to calculate the convection cooling rate of 0.94 MW/m^2. As the heat flux rate from internal nuclear heating is greater than the convection cooling rate, the FW panel will increase in temperature until an equilibrium is reached.

8 References

(2019, January 25). Retrieved from Iter Website: https://www.iter.org/

A. A. Badawi, h. I. (2004). *Thermal Analysis Of The ITER Blanket First Wall.* Cairo: Physics Dept., Science Faculty, Ain Shams University, Cairo, Egypt.

A.A. Suvorova, I. D. (2018). Heat treatment effects on the microstructure and properties of Cu–Cr–Zr alloy used for the ITER blanket components. *Nuclear Materials and Energy*, 80-84.

Alfredo Ferrari, P. R. (2018). *Fluka: a multi-particle transport code.* Geneva: CERN EUROPEAN ORGANIZATION FOR NUCLEAR RESEARCH.

Barbarino, M. (2018, September 19). *Fusion Energy in the 21st Century: Status and the Way Forward*. Retrieved from IAEA: https://www.iaea.org/newscenter/news/fusion-energy-in-the-21st-century-status-and-the-way-forward

Bennet, D., & Thomson, J. (1989). *The Elements of Nuclear Power.* United States: Longman.

Boron 10. (2019, December 28). Retrieved from nuclear-power.net: https://www.nuclear-power.net/glossary/boron-10/

Castle Bravo. (2020, January 2). Retrieved from wikipedia.org: https://en.wikipedia.org/wiki/Castle_Bravo#Cause_of_high_yield

Culham Centre for Fusion Energy. (2020, September 12). Retrieved from UK Atomic Energy Authority: https://ccfe.ukaea.uk/research/joint-european-torus/

D.A. Brown, M. C. (2018). ENDF/B-VIII.0: The 8th Major Release of the Nuclear Reaction Data Library with CIELO-project Cross Sections, New Standards and Thermal Scattering Data, Nuclear Data Sheets, 148: pp. 1-142.

Dombrowski, D. E. (1996). *Manufacture of beryllium for fusion energy applications .* Cleveland: Fusion Engineering and Design.

Haeck, W. P. (2017). *A Comparison of Monte Carlo and Deterministic Solvers for keff and Sensitivity Calculations.* Los Alamos: Los Alamos National Laboratory.

Heat Generation. (2019, December 28). Retrieved from nuclear-power.net: https://www.nuclear-power.net/nuclear-engineering/heat-transfer/heat-generation/

Hutton, T. (2019, October 24). Parsed FLUKA output file. University of Cape Town.

Krane, K. S. (1988). *Introductory Nuclear Physics.* John Wiley & Sons Inc.

Lewis, E. E. (2008). *Fundamentals of Nuclear Reactor Physics.* Evanston, Illinois: Elsevier Academic Press.

Lilley, J. (2001). *Nuclear Physics - Principles and Applications.* John Wiley and Sons Ltd.

M.R. Gilbert and J.-Ch. Sublet. (2011). Neutron-induced transmutation effects in W andW-alloys in a fusion environment. *NUCLEAR FUSION*.

M.R. Gilbert, S. D.-C. (2012). An integrated model for materials in a fusion power plant: transmutation, gas production, and helium embrittlement under neutron irradiation. *NUCLEAR FUSION*.

McMorrow, D. (2011). *Tritium.* McLean, Virginia: The MITRE Corporation.

Nuclear fusion. (2019, January 10). Retrieved from Wikipedia.org: https://en.wikipedia.org/wiki/Nuclear_fusion

Peterson, S. (2018). *EEE4106Z Radiation Interactions & Detection.* Cape Town: University of Cape Town.

Popov, E. a. (2011). Modeling and Simulation of the ITER First Wall/Blanket Primary Heat Transfer System. *Fusion Science and Technology*, 128-133.

R.B. Firestone, S. M. (2007). *Database of Prompt Gamma Rays from Slow Neutron Capture for Elemental Analysis.* Vienna: INTERNATIONAL ATOMIC ENERGY AGENCY.

Technical Developments for Harnessing Controlled Fusion. (2011). In S. Z. G. Veres, *Handbook of Nuclear Chemistry* (p. 2792). Germany: Springer Science+Business Media B.V. 2011.

Tomberlin, T. A. (2004). Beryllium – A Unique Material In Nuclear Applications. *36th International SAMPE Technical Conference* (p. 12). Idaho Falls: Idaho National Engineering and Environmental Laboratory.

9 Appendices

9.1 Appendix A: Mass Defect Energy

Calculating the Q-value of the D-T fusion reaction.

From (Bennet & Thomson, 1989) Table 1.1 provides us the rest mass of a proton, neutron and electron:

	Mass (u)	Electronic Charge
Proton (p)	1.007277	+1
Neutron (n)	1.008665	0
Electron (e)	0.00055	-1

From (Bennet & Thomson, 1989) Table 1.2 provides us the rest mass of some isotopes:

Isotope	Mass (u)
Hydrogen (^{1}H)	1.007825
Deuterium (^{2}H)	2.01410
Tritium (^{3}H)	3.01605
Helium (^{4}He)	4.00260

The D-T fusion reaction is as follows:

$^{3}_{1}\mathrm{H} + ^{2}_{1}\mathrm{H} \rightarrow ^{4}_{2}\mathrm{He} + ^{1}_{0}\mathrm{n}$ + MD

3.01605u + 2.01410u → 4.00260u + 1.008665u + MD

5.03015u → 5.011265u + MD

A mass defect of 0.018885u was calculated in the reaction

0.018885u x 1.6604x10^{-27} kg = 3.1356654 x10^{-29} kg

The equivalence between mass and energy is expressed by the famous equation:

$E = mc^2$

E = (3.1356654 x10^{-29} kg) x (2.998 m/s)^2 = 2.818337316 x 10^{-12} J

Converting to eV:

2.818337316 x 10^{-12} J / 1.602 x10^{-19} J/eV = <u>17.59 MeV</u>

9.2 Appendix B: Energy of fusion products

Neglecting kinetic energies of reacting particles before fusion which is justified by the fact that those energies are usually in the 1-10keV range and fusion yield is in the MeV range. In the CM (Centre of Mass) frame the energies of constituents a and b in terms of fusion energy release Q are:

$$½m_av_a^2 + ½m_bv_b^2 = Q$$

The magnitude of the momenta in that frame are equal:

$$m_av_a = m_bv_b$$

Combining the equations gives:

$$½m_av_a^2 = Q/(1 + m_a/m_b) \; ; \; ½m_bv_b^2 = Q/(1 + m_b/m_a)$$

This allows us to determine the relative magnitudes of energies of the two fusion products:

$$½m_av_a^2 / ½m_bv_b^2 = m_b/m_a$$

For the D-T fusion, the energy released is Q = 17.59 MeV

The total rest mass energy for the helium ion ($^4_2\mathrm{He}$) is as follows:

$m(^4_2\mathrm{He}) = 4.00260u = 4.00260 \times 1.6604 \times 10^{-27}kg$

$= 6.64591704 \times 10^{-27}$ kg

$E_a = mc^2 \; ; \; m = E/c^2 \; ; \; m_a = 5.5973352894 \times 10^{-10}$ J / [1.602×10^{-19} J/eV] x c^2

$m_a = 3.7286$ GeV / c^2

The total rest mass energy for the fusion neutron ($^1_0\mathrm{n}$) is as follows:

$m(^1_0\mathrm{n}) = 1.008665u = 1.008665 \times 1.6604 \times 10^{-27}kg$

$= 1.674787366 \times 10^{-27}$ kg

$E_b = mc^2 \; ; \; m = E/c^2 \; ; \; m_b = 1.505299554 \times 10^{-10}$ J / [1.602×10^{-19} J/eV] x c^2

$m_b = 0.9396$ GeV / c^2

The ratio of the energies of the fusion products is as follows:

$$E_a / E_b = ½m_av_a^2 / ½m_bv_b^2 = m_b/m_a$$

$E_a / E_b = [0.9396$ GeV / $c^2] / [3.7286$ GeV / $c^2] = 0.25199$

Since $E_a + E_b = Q = 17.59$ MeV ; $0.25199 \times E_b + E_b = 17.59$ MeV

Then $E_b = 17.59$ MeV / 1.25199 = <u>14.0496 MeV for fusion neutron</u>

Then $E_a = 0.25199 \times 14.0496$ MeV = <u>3.540 MeV for helium ion</u>

9.3 Appendix C: Flair input file (Screenshot)

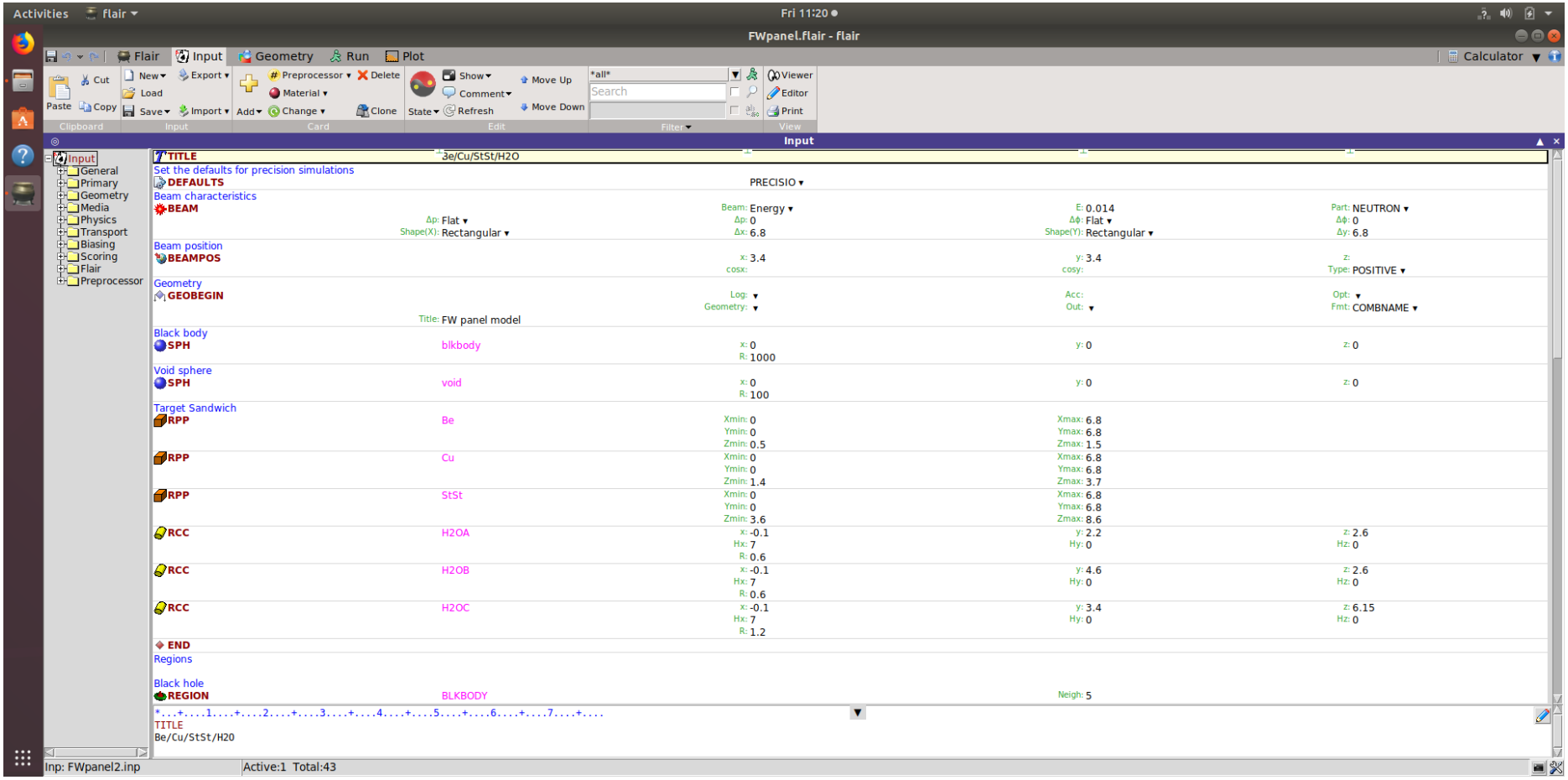

9.4 Appendix D: Flair geometry view (Screenshot)

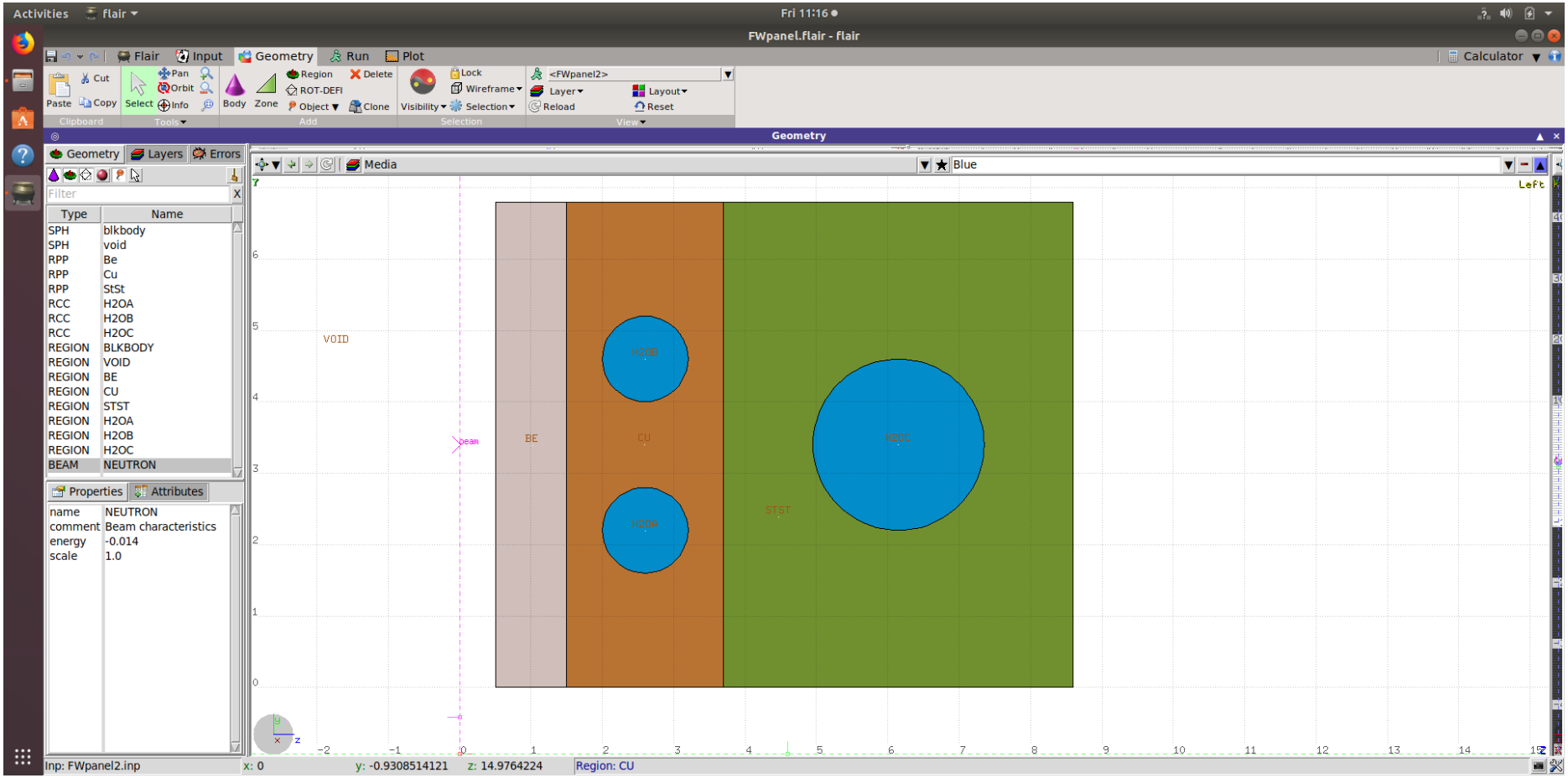

9.5 Appendix E: Flair geometry in 3-dimensions with cut away (Screenshot)